NAIST-IS-DD1561031

Doctoral Dissertation

Channel Estimation and Detection for Advanced Digital Terrestrial Television System

Ryan Paderna

March 15, 2018

Graduate School of Information Science
Nara Institute of Science and Technology

A Doctoral Dissertation
submitted to Graduate School of Information Science,
Nara Institute of Science and Technology
in partial fulfillment of the requirements for the degree of
Doctor of ENGINEERING

Ryan Paderna

Thesis Committee:

Professor Minoru Okada	(Supervisor)
Professor Kenji Sugimoto	(Co-supervisor)
Associate Professor Takeshi Higashino	(Co-supervisor)
Assistant Professor Duong Quang Thang	(Co-supervisor)
Assistant Professor Yafei Hou	(Co-supervisor, Okayama University)

Channel Estimation and Detection for Advanced Digital Terrestrial Television System*

Ryan Paderna

Abstract

The research contributions are to improve both capacity and reliability for next generation broadcasting systems. Due to spectrum-scarcity, the capacity improvement for new services, e.g., 4K television, requires radio broadcasting signals using the same frequency band as the existing Integrated Services Digital Broadcasting - Terrestrial (ISDB-T). To fulfill this task, we employ Layered Division Multiplexing (LDM) to simultaneously transmit: (1) primary data stream for ISDB-T and (2) an additional secondary data stream, from which 4K receiver can combine with the primary stream to obtain 4K signal. In doing so, an interference problem between two data streams arises which may result in a severe reliability deterioration for both layers. Therefore, we only multiplex the secondary stream in a partial manner so that the interference between layers can be reduced. Partial LDM is possible since the transmission capacity of the secondary layer exceeded the minimum requirement due to reuse of primary layer. We can reduce the error-rate using partial LDM because there will be less interference between two layers of LDM.

Improving the reliability for broadcasting systems requires accurate knowledge of the radio channel, which can be acquired by channel estimation (CE) process. Since the impulse response of the radio channel is sparse, we adopt compressed sensing (CS) to efficiently perform the CE. The CS-based CE generates the channel impulse response by initially determining the delay time for each path and then calculating the associated attenuation coefficients. Therefore, CS-based CE

*Doctoral Dissertation, Graduate School of Information Science,
Nara Institute of Science and Technology, NAIST-IS-DD1561031, March 15, 2018.

is vulnerable to fractional delay where the delay time cannot be correctly recovered due to long sampling period and/or imperfect synchronization in broadcasting systems. Therefore, we have proposed a "virtual oversampling" technique for CS which uses an oversized Discrete Fourier Transform (DFT) matrix to detect the fractional delay at the receiver-side without increasing the signal bandwidth. As a result, accuracy of the CE and the reliability of the transmission are significantly improved.

Keywords:

Compressed sensing, Orthogonal Matching Pursuit, ISDB-T, DTTB, LDM, SFN, STBC

Contents

List of Figures

1 Introduction

The first part of this chapter discusses the research motivation of LDM and CS in DTTB system. And then, the statement of the problem of the dissertation is presented. Next, the research contribution and scope will be discuss. The dissertation layout is shown at the last part of this chapter.

1.1 Research Motivation

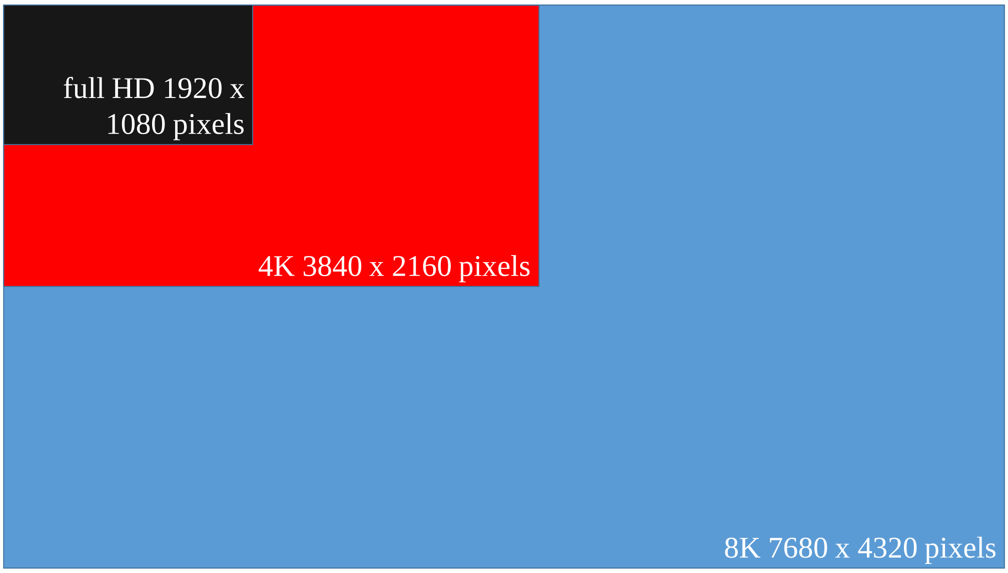

Figure 1.1: The resolution comparison between full HD, 4K and 8K

Television broadcasting is popular all throughout the world. In fact, there are over 1.4 billion television sets and 4.9 billion television audience in the world around 2009 alone, according to the statistics from International Telecommunications Union (ITU) [6]. That is because television provides much information and entertainment aside from newspapers, radio, and Internet. With the development of technology and innovation, television system evolves throughout the years from black and white to color, and from analog to digital. Currently, television will evolve from HDTV to 4K/8K resolution. Figure 1.1 shows the resolution comparison between full HD, 4K, and 8K. Here we can see that 4K/8K has higher resolution compared to the previous full HD resolution. With the high resolution for 4K/8K, the viewers can enjoy almost close to reality videos compared to full HD resolution. Most of the household today preferred to have 4K TV instead of 8K TV because the size of 8K TV is too big. 8K TV is only popular for advertisement screens in public places such as airport, malls, train stations, etc.

The delivery of the television services to the people is now very flexible. People can now access television program in many ways such as terrestrial DTV, satellite DTV, cable DTV, and Internet Protocol TV (IPTV). Nevertheless, terrestrial DTV is still the most popular because the infrastructure implementation is easy, and the terrestrial signal is free for all. There are many standards for DTTB system around the world which includes Digital Video Broadcasting-Terrestrial (DVB-T) [7], Advanced Television System Committee (ATSC) [8], Integrated Services Digital Broadcasting-Terrestrial (ISDB-T) [2], and Digital Terrestrial Multimedia Broadcasting (DTMB) [9]. In Japan, ISDB-T is currently used since 2003 after analog broadcasting. In fact, analog broadcasting was completely shutdown last 2011. And at the moment, 4K/8K terrestrial broadcasting is currently on going development which is the next step after ISDB-T.

Because of the evolution of TV system, the new system always require higher transmission capacity compared to older generation DTTB system. However, the transmission capacity is very limited and cannot support higher transmission demand for 4K/8K TV sets. Fortunately, there are many researches and methods to improve the signal detection and transmission efficiency. Nowadays, hardwares is capable of faster processing with high memory which can support complex signal processing. The multiplexing of signals before is only limited to either time division multiplexing and frequency division multiplexing. With the advent of improved error correcting codes, we can now transmit multiple information at the same time and at the same frequency spectrum resources using Layered Division Multiplexing (LDM) [10]. With LDM, the transmission capacity will increase which can be applied for next generation DTTB system for 4K/8K TV.

However, terrestrial wireless broadcasting comes with a price because the signal suffers from interference and multi-path propagation that degrades the signal quality when the signal reaches the receiver. One way to improve the signal quality is to estimate the channel itself. Since broadcast transmission is always from transmitter to receiver without any feedback, the transmitter will use pilot for a receiver to know the quality of the channel. That is why, CE is very important in the field of wireless broadcasting. With various studies about wireless channel, it was found out that the channel has a sparse characteristic [11–14]. Because of the assumption that wireless channel is a sparse, the channel estimation always consider the method called compressed sensing (CS). CS is very beneficial because it only requires few pilots and the overall performance is better resulting to higher transmission capacity [15].

1.2 Statement of the Problem

The demand of DTTB transmission capacity is increasing overtime. It is very necessary to develop a new technology that will support higher transmission capacity over wireless channel. For the next generation DTTB system, the transmission capacity should support a 4K resolution transmission. Implementing a 4K terrestrial broadcasting is very challenging because there are no available frequency spectrum, and it also requires high transmission capacity. Since the next generation DTTB system does not have enough frequency spectrum resources, this research will reuse the frequency spectrum resources of ISDB-T.

Another issue to consider is how to increase the wireless transmission efficiency. For OFDM to have better transmission efficiency, the majority contents of subcarriers should be data (video or audio) instead of pilots for CE. That is why, CS was considered as a technique for CE because it only requires less pilots with better overall performance [16]. However, CS requires higher complexity in estimating the channel.

One of the technique of complexity reduction for CS based CE is to implement in time domain instead of frequency domain [17]. The frequency domain CE is considered to be high in complexity because the system requires CE for each

OFDM subcarrier. The total number of OFDM subcarrier for DTTB system is enormously high which makes it difficult to implement CE for all OFDM subcarriers. In time domain CE, we only need to estimate the CIR within the guard interval which is less complex compared to frequency domain CE.

However, time domain CE suffers from the impact of fractional delay due to non-synchronization between transmitter and receiver [18]. With the fractional delay, the CIR will be no longer sparse which makes CIR estimation difficult using CS. One of the solution to lessen the impact of fractional delay is to apply oversampling [19]. However, oversampling will further increase the transmission bandwidth and the ISDB-T is only limited to 6MHz. This research considers the problem of fractional delay for time domain CE. In addition, the problem should also consider the complexity requirement in reducing the impact of fractional delay.

1.3 Research Contribution

The first contribution is the system design to increase the transmission capacity of ISDB-T to be used in next generation DTTB system which is related to publication (J1) and (D1). In this topic, the researcher implements a LDM to transmit additional data to scale up the ISDB-T into 4K resolution. In addition, the proposed system implements only partial LDM to lessen the interference between the ISDB-T and the additional data since the conventional full LDM already exceeds the minimum transmission capacity for 4K system.

The second contribution of the dissertation is the time domain channel estimation using compressed sensing. In time domain CE, a fractional delay issue arises when a receiver is no longer synchronized with the transmitter. To lessen the impact of fractional delay, the researcher proposes a virtual oversampling as a substitute of oversampling since oversampling will increase the transmission bandwidth. In addition, this research modifies the algorithm of CS called Orthogonal Matching Pursuit (OMP) to lessen the computational cost in estimating the channel.

The second contribution is divided into two sub-contributions. The first is the mitigation of fractional delay which is related to journal publication (J2) and domestic conference publication (D2). The other sub-contribution of the second contribution is about low-complexity channel estimation which is related to international conference publication (I1) and (I2), and domestic conference publication (D3).

1.4 Scope and Limitation

The scope of this research includes the theoretical design of the components of transmitter and receiver of DTTB system. The first task includes the formation of signal model from transmitter to receiver. The signal model can be described in two parts which includes transmitted signal, and the received signal. The low complexity channel estimator and detector scheme are included in the receiver side. The second task is the implementation of the designed model using simulations. The simulation results include the BER performance of the proposed systems. The research is limited and does not include the actual hardware implementation of the transmitter and receiver.

1.5 Dissertation Layout

The dissertation is divided into six chapters. Chapter 1 presents the introduction that includes motivation, statement of the problem, contributions, and limitations of the research. Chapter 2 discusses the overview and system model of ISDB-T and next generation DTTB system. In Chapter 2, the signal model was described in terms of transmitted signal and received signal. Chapter 3 presents the proposed migration of next generation DTTB system using LDM. Chapter 4 contains the detailed discussion about time domain CE for ISDB-T and next generation DTTB system using CS. The first part of Chapter 4 contains the overview of CS. And then, the channel estimator of ISDB-T and next generation DTTB system will be discussed in detail in the last part of Chapter 4. Chapter 5 presents the proposed low complexity channel estimator using CS with virtual oversampling. Finally, the last chapter will conclude the dissertation.

Table 1.1 shows the corresponding publications that is link to different chapters of this dissertation. The publication reference is referred to the publication list

Table 1.1: Dissertation chapters with its corresponding publications

	J1	J2	I1	I2	D1	D2	D3
chapter 2			○	○			
chapter 3	○				○		
chapter 4			○	○			○
chapter 5		○				○	

of the dissertation.

2 Overview of Digital Terrestrial Television Broadcasting

2.1 Integrated Services Digital Broadcasting - Terrestrial

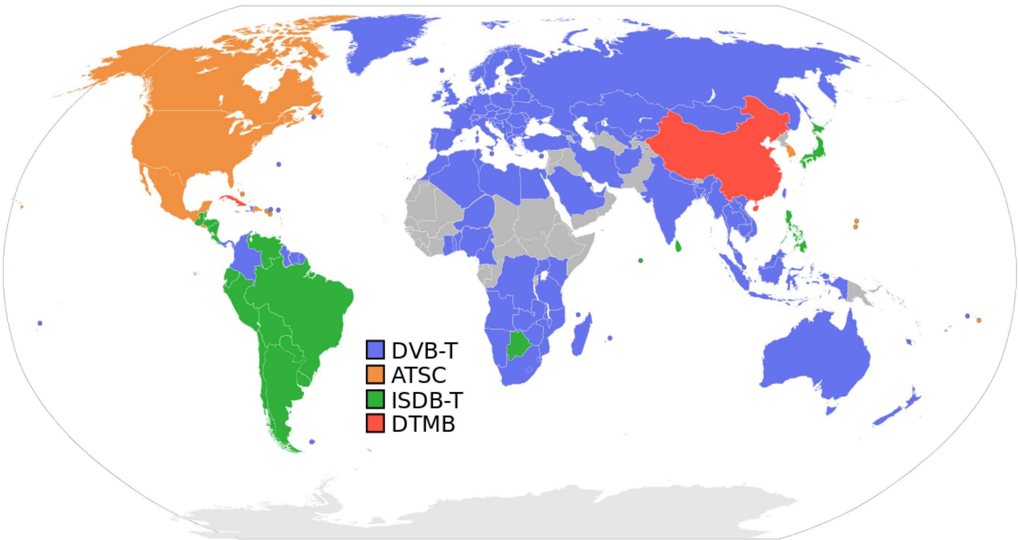

Figure 2.1: DTTB standards around the world [1]

ISDB-T is a Japanese standard for DTTB system that was implemented in Japan since 2003 [2]. Other countries around the world such as Philippines, South America, Sri Lanka, etc. also adopted the ISDB-T. Figure 2.1 shows the DTTB standards around the world. ISDB-T is capable of offering different services such as television, mobile TV, emergency notification for earthquake, tsunami, etc.

Table 2.1: Parameters of the ISDB-T standard

ISDB-T mode	Mode 1	Mode 2	Mode 3
Number of OFDM segments	13		
Channel bandwidth	6 MHz		
Useful bandwidth	5.575 MHz	5.573 MHz	5.572 MHz
Subcarrier spacing	3.968 kHz	1.984 kHz	0.9992 kHz
Number of total subcarriers	1405	2809	5617
Number of data subcarriers	1248	2496	4992
Modulation method	DPSK, QPSK, 16QAM, 64QAM		
FFT window size	2048	4096	8192
Number of symbols per frame	204		
Effective symbol length	252 μs	504 μs	1008 μs
Guard interval length	1/4,1/8,1/16,1/32 of effective symbol length		
Inner code	Convolutional code (1/2, 2/3, 3/4, 5/6, 7/8)		
Outer code	Reed-Solomon (204,188)		

The ISDB-T uses multiple subscarriers in frequency domain to transmit symbols. This modulation technique is so-called "OFDM". The Orthogonal Frequency Division Multiplexing (OFDM) is a broadband modulation scheme transmitting a high rate stream using multiple subcarriers with low symbol rate [20]. The OFDM has many merits such as high spectral efficiency, and robust against intersymbol interference. The spectral efficiency of OFDM is very high because it does not require any guard bands in between the subcarriers. In addition, each subcarrier is so narrow enough to make it prone to frequency-selective channels. In such transmission system, each subcarrier experiences a random flat fading while the whole signal spectrum experiences frequency selective fading. Thus, reliable estimation for channel frequency response (CFR) is necessary for accurate signal detection. OFDM is also prone to multipath fading due to the guard interval inserted in front of every OFDM symbol [21].

ISDB-T offers three different modes depending on the trade off between multipath fading and Doppler shift. Table 2.1 shows the different parameters for each different mode. Mode 1 is mostly used for mobile reception because it is robust against Doppler shift due to small symbol length. On the other hand, Mode 3 can be implemented for fixed receiver because it is robust against multipath fading due to longer symbol length. While mode 2 is neutral or in between mode 1 and mode 3. These modes are selected depending on channel characteristic and receivers which offers great flexibility to different scenarios.

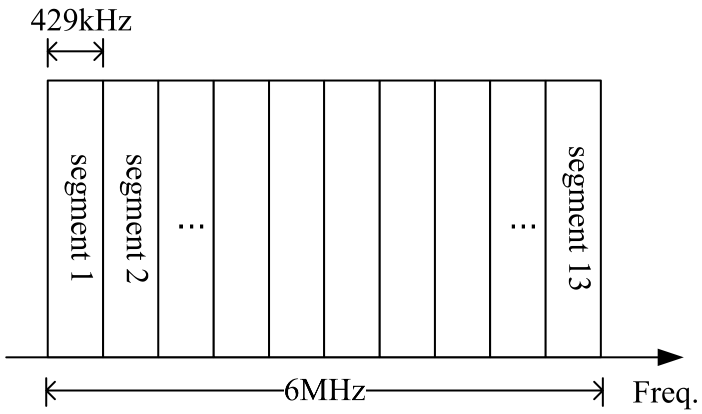

Figure 2.2: 13 segments of ISDB-T

In ISDB-T, a 6MHz bandwidth is divided into 13 segments as shown in Fig. 2.2. Each segment has a bandwidth approximately 429 kHz. And also, each segment has an independent parameters, coding rate, and modulation scheme. Segmentation of ISDB-T bandwidth will allow a partial reception for different types of receiver. For example, a mobile receiver will only use single segment, while fixed receiver will require more than one segment. With this kind of bandwidth segmentation, only single 6MHz of bandwidth of ISDB-T is needed for all types of receiver eg. fixed receiver or mobile receiver.

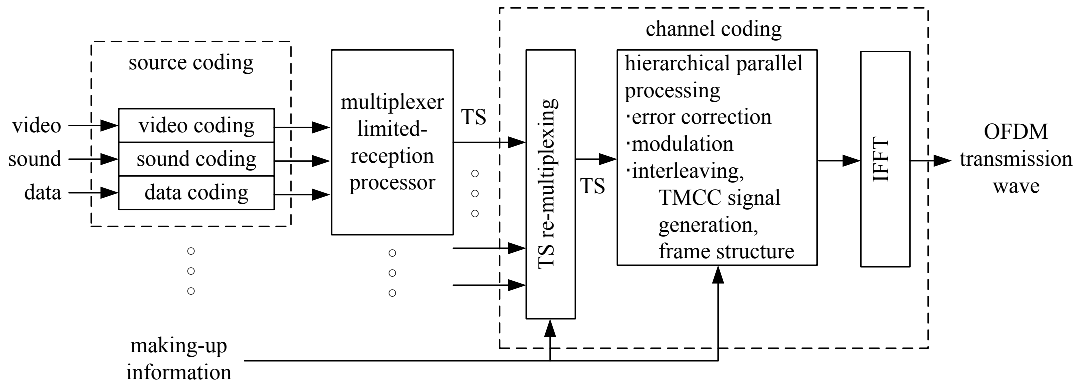

Figure 2.3: Overview of the signal processing in ISDB-T transmitter [2]

Figure 2.3 shows the overview of ISDB-T transmitter. The video, sound, and the other data are encoded as an "MPEG-2 systems" in the source coding block for initialization. The MPEG-2 systems are then re-multiplexed to create a single transport stream (TS) to the channel coding. Finally, the signal is then sent as a single OFDM transmission wave after channel coding. The ISDB-T can provide standard-definition TV (SDTV), high-definition TV (HDTV), one-seg mobile reception for handheld devices, interactive TV, and emergency warning broadcasting. The signal power requirement for ISDB-T transmission is lesser compared to analog TV.

2.1.1 System model of conventional ISDB-T

Figure 2.4 shows the system block diagram for the transmitter and receiver of ISDB-T. The payload **u** is composed of $(K - M)$ data symbols and M pilot symbols inserted in OFDM subcarriers. The arrangement of the pilots and data subcarriers are shown in Fig.2.5. The payload **u** is defined as,

$$\mathbf{u} = \begin{bmatrix} u_0 & u_1 & \cdots & u_{K-1} \end{bmatrix}^T, \tag{2.1}$$

where $[\cdot]^T$ is transpose of a vector. The entry payload vector **u** is defined as

$$u_{Cm+i} = \begin{cases} p_m & ; (i = 0) \\ d_{Cm+i} & ; (0 < i < C). \end{cases} \tag{2.2}$$

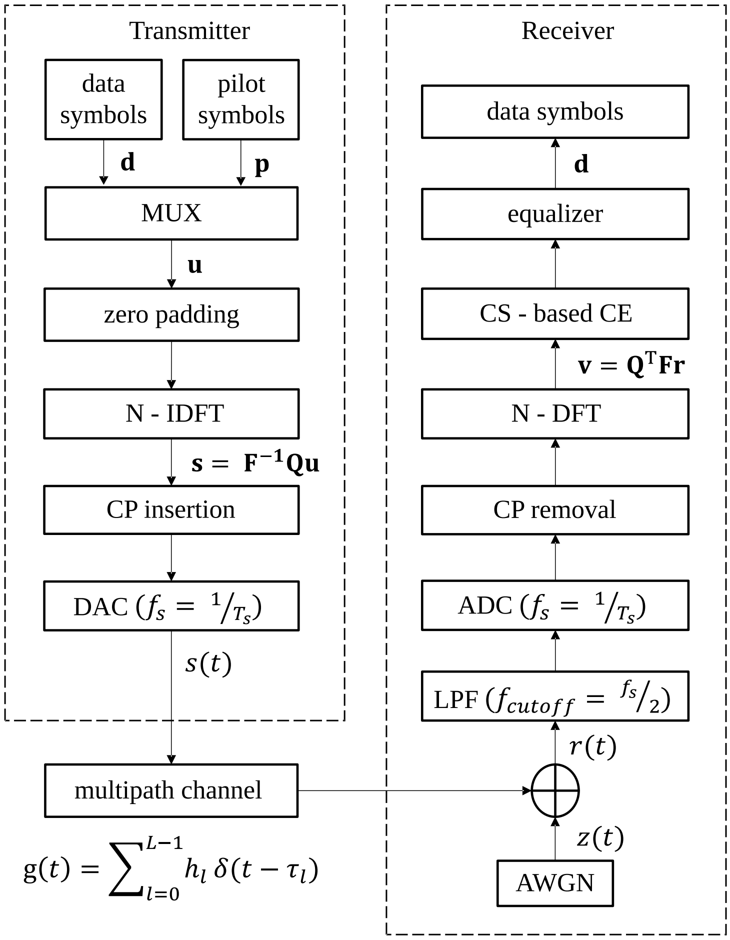

Figure 2.4: ISDB-T system block diagram for transmitter and receiver

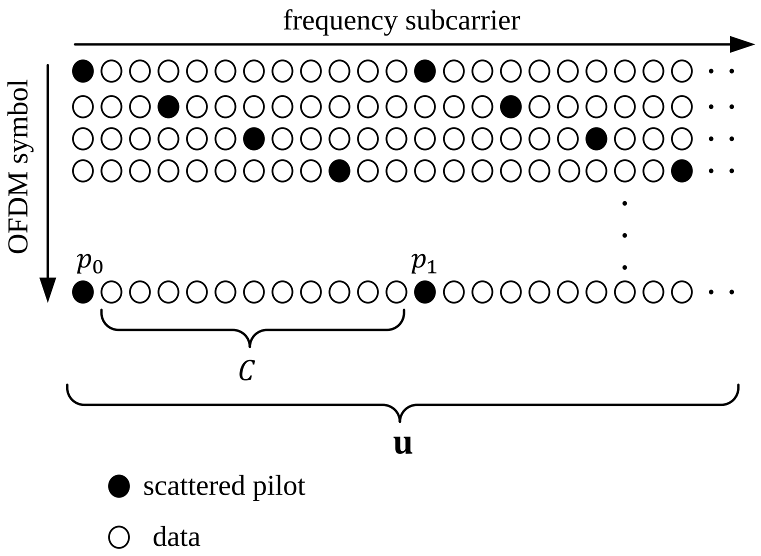

Figure 2.5: Subcarrier arrangement for pilot and data symbol of OFDM for ISDB-T

The p_m is the m-th pilot symbol where $m \in \{0, ..., M-1\}$ and d_{Cm+i} is the $(Cm+i)$-th data symbol. The $C = \text{round}(K/M)$ represents the number of data subcarriers inserted between the two pilots.

The OFDM symbol $\mathbf{s}$ can now be obtained by multiplying the payload $\mathbf{u}$ with the reordering matrix $\mathbf{Q}$ and the inverse of DFT matrix $\mathbf{F}$ defined as

$$\mathbf{s} = \mathbf{F}^{-1}\mathbf{Q}\mathbf{u}. \tag{2.3}$$

The reordering matrix $\mathbf{Q}$ is defined as

$$\mathbf{Q} = \begin{bmatrix} \mathbf{0}_{(K/2)\times(K/2)} & \mathbf{I}_{K/2} \\ \mathbf{0}_{(N-K)\times(K/2)} & \mathbf{0}_{(N-K)\times(K/2)} \\ \mathbf{I}_{K/2} & \mathbf{0}_{(K/2)\times(K/2)} \end{bmatrix}, \tag{2.4}$$

with a size of N by K. The structure of reordering matrix is composed of identity matrix $\mathbf{I}_K$ with size of K and zero matrix $\mathbf{0}_{K\times N}$ with size of K by N. The purpose of reordering matrix is to arrange the positive side and negative side of active OFDM subcarriers. While the matrix $\mathbf{Q}$ will suppress the unused subcarriers before actual transmission. The DFT matrix $\mathbf{F}$ with size N by N is defined as

$$\mathbf{F} = \frac{1}{\sqrt{N}} \left[\exp\left(-j \frac{2\pi kn}{N} \right) \right]_{\substack{0 \le k < (N-1) \\ 0 \le n < (N-1)}} . \tag{2.5}$$

A cyclic prefix (CP) is added to $\mathbf{s}$ to avoid inter-symbol interference. And then, the signal is applied to the digital-to-analog converter (DAC) to generate the baseband transmit signal $s(t)$. Bandwidth of the DAC is $f_s = 1/T_s$ where T_s is symbol interval. Here we can observed that oversampling is not applied in the transmitter side. The OFDM symbol $\mathbf{s}$ is then up-converted and transmitted. During transmission, an additive white Gaussian noise is added to the transmitted signal together with multipath channel.

At the receiver side, the received signal is initially frequency down-converted using low pass filter after convolution operation with $g(t)$ defined as

$$r(t) = g(t) * s(t) + z(t), \tag{2.6}$$

where $g(t)$, $z(t)$ are the channel impulse response (CIR) and AWGN, respectively. The operation $(*)$ denotes convolution. The CIR is expressed as

$$g(t) = \sum_{l=0}^{L-1} h_l \delta(t - \tau_l) \tag{2.7}$$

where h_l is complex-valued gain and τ_l is the delay for the l-th propagation path of the L multipath channel.

The received signal, $r(t)$, is applied to a low pass filter with a cut-off frequency of $1/(2T_s)$, followed by the analog-to-digital (ADC) converter with sampling frequency $f_s = 1/T_s$. And then, CP removal is performed after from the analog-to-digital conversion .

The received signal $\mathbf{r}$ after CP removal is then given by

$$\mathbf{r} = \mathbf{G}\mathbf{s} + \mathbf{z}, \tag{2.8}$$

where $\mathbf{G}$ and $\mathbf{z}$ represent the channel matrix in time domain and the noise vector, respectively.

We observed that the signal processing in the receiver is the opposite of the transmitter and uses the same DFT matrix $\mathbf{F}$ and transpose of reordering matrix

Table 2.2: Specification of next generation DTTB system using MIMO transmission [22]

Modulation method	OFDM
Occupied bandwidth	5.57 MHz
Carrier modulation	64QAM, 256QAM, 1024QAM, 4096QAM
FFT size	8k (5,617), 16k (11,233), 32k (22,465), 64k (44,929)
Guard interval ratio	1/8 (504 μsec), 1/16 (252 μsec), 1/32 (126 μsec)
Error-correcting code	inner:LDPC (code rate →2/3, 3/4, 5/6), outer:BCH
Transmission capacity	91.8 Mbps (4096QAM), 76.5Mbps (1024QAM)

$\mathbf{Q}$ of the transmitter. The received signal vector $\mathbf{v}$ in frequency domain can be obtained using

$$\mathbf{v} = \mathbf{Q}^T\mathbf{F}\mathbf{r} = \mathbf{Q}^T\mathbf{H}\mathbf{Q}\mathbf{u} + \mathbf{z}_F, \tag{2.9}$$

where $\mathbf{H} = \mathbf{F}\mathbf{G}\mathbf{F}^{-1} = \mathrm{diag}(\mathbf{h}_f)$ is the diagonal frequency domain channel matrix. The diagonal elements of $\mathbf{H}$ forms the channel frequency response $\mathbf{h}$, where each entry is

$$h\Big(\frac{n}{NT_s}\Big) = \sum_{l=0}^{L-1} h_l \exp\Big(-j\frac{2\pi n\tau_l}{NT_s}\Big), \Big(0 \leq n < (N-1)\Big). \tag{2.10}$$

While the $\mathbf{z}_F = \mathbf{Q}^T\mathbf{F}\mathbf{z}$ is the noise spectrum.

2.2 Next Generation DTTB System

The next generation DTTB system will implement 8K/4K terrestrial broadcasting. It uses several new technologies such as Multiple Input Multiple Output (MIMO), Single Frequency Network (SFN), and STBC to support high transmission rate requirements for 8K/4K Ultra High Definition TV (UHDTV). Table 2.2 shows several parameters for the next generation DTTB with a transmission capacity up to 91.8 Mbps. This kind of transmission can perfectly support an 8K transmission using only 6MHz of bandwidth.

At the moment, the next generation DTTB system is on going development because there are not much frequency spectrum resources to support a terrestrial broadcasting. This is the reason why the developers consider an SFN technique for frequency spectrum reuse in every transmitter. SFN is a network of transmitters that transmit signals using single frequency spectrum resources to widen the coverage area [23].

2.2.1 System model of next generation DTTB system

Figure 2.6 presents the system model of next generation DTTB system using SFN. The system model in the shown figure is composed of two transmitters (transmitter A and transmitter B) that transmit the same set of signals with synchronization. Each transmitter and receiver is composed of two antennas (horizontal and vertical). The whole system is equivalent to a 4x2 MIMO system with a channel defined as $h_{i,j}$ from j-th antenna of the transmitter to i-th antenna of the receiver. The location of the two transmitters are separated in different location with different coverage area. In Fig.2.6, the location of the receiver is within the overlapping coverage area of two transmitters wherein the receiver receives signals from both transmitters. The pair of transmitters should synchronized with each other using STBC to avoid intersymbol interference between the signals of different transmitters.

Table 2.3: Transmission of symbols using STBC

	transmitter A		transmitter B	
time	horizontal	vertical	horizontal	vertical
t	S_0	S_1	$-S_2^*$	S_3^*
$t+1$	S_2	S_3	S_0^*	$-S_1^*$

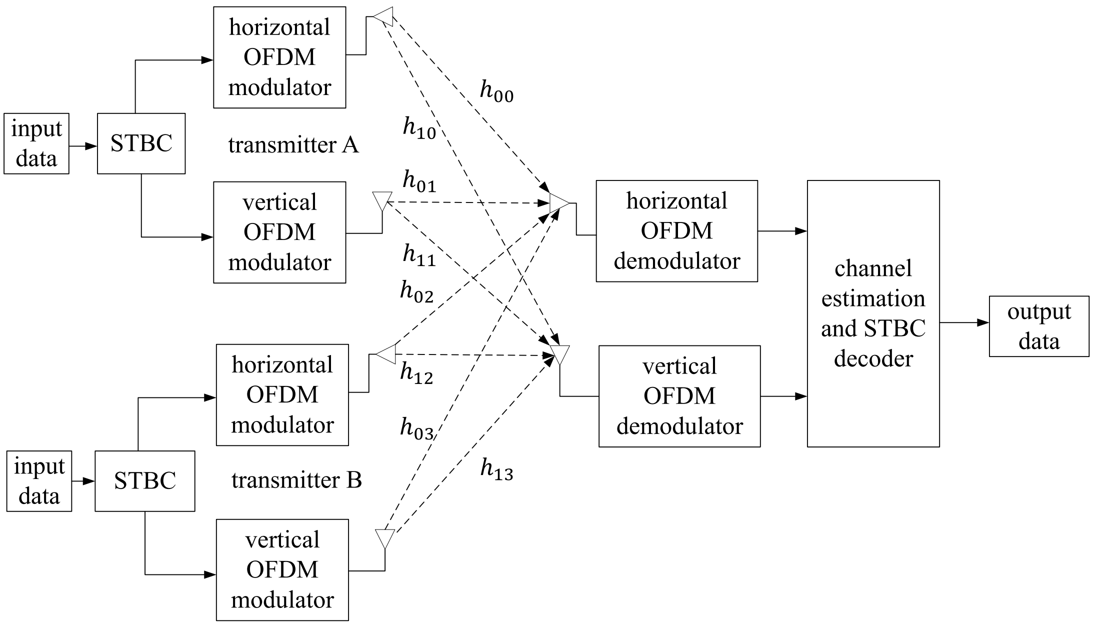

Figure 2.6: System model of next generation DTTB system using SFN [3]

The STBC is a multiplexing technique for wireless communications using multiple antennas [24]. The STBC can increase the diversity without requiring any bandwidth expansion and it does not require feedback from receiver to the transmitter. For example, if we are given a symbols $\{S_0, S_1, S_2, S_3\}$ for transmission, the STBC will require two time instances (t and $t+1$) for complete transmission of the symbols. Table 2.3 shows the symbols to be transmitted in each antenna in every time instances. The notation $(\cdot)^*$ indicates the complex conjugate of the symbol.

Using the transmitted symbols in table 2.3, the received signal in horizontal antenna $y_0^{(t)}$ and vertical antenna $y_1^{(t)}$ at time instant t can be modeled as

$$\begin{bmatrix} y_0^{(t)} \\ y_1^{(t)} \end{bmatrix} = \begin{bmatrix} h_{00}^{(t)} & h_{01}^{(t)} & h_{02}^{(t)} & h_{03}^{(t)} \\ h_{10}^{(t)} & h_{11}^{(t)} & h_{12}^{(t)} & h_{13}^{(t)} \end{bmatrix} \begin{bmatrix} S_0 \\ S_1 \\ -S_2^* \\ S_3^* \end{bmatrix}, \tag{2.11}$$

while the received signal at time instant $t+1$ can be modeled as,

$$\begin{bmatrix} y_0^{(t+1)} \\ y_1^{(t+1)} \end{bmatrix} = \begin{bmatrix} h_{00}^{(t+1)} & h_{01}^{(t+1)} & h_{02}^{(t+1)} & h_{03}^{(t+1)} \\ h_{10}^{(t+1)} & h_{11}^{(t+1)} & h_{12}^{(t+1)} & h_{13}^{(t+1)} \end{bmatrix} \begin{bmatrix} S_2 \\ S_3 \\ S_0^* \\ -S_1^* \end{bmatrix}. \tag{2.12}$$

By combining the Eq.(2.11) and Eq.(2.12), we can have an equivalent 4x4 MIMO system described as

$$\begin{bmatrix} y_0^{(t)} \\ y_1^{(t)} \\ y_0^{*(t+1)} \\ y_1^{*(t+1)} \end{bmatrix} = \begin{bmatrix} h_{00}^{(t)} & h_{01}^{(t)} & h_{02}^{(t)} & h_{03}^{(t)} \\ h_{10}^{(t)} & h_{11}^{(t)} & h_{12}^{(t)} & h_{13}^{(t)} \\ h_{02}^{*(t+1)} & -h_{03}^{*(t+1)} & -h_{00}^{*(t+1)} & h_{01}^{*(t+1)} \\ h_{12}^{*(t+1)} & -h_{13}^{*(t+1)} & -h_{10}^{*(t+1)} & h_{11}^{*(t+1)} \end{bmatrix} \begin{bmatrix} S_0 \\ S_1 \\ -S_2^* \\ S_3^* \end{bmatrix}. \tag{2.13}$$

The channel matrix in Eq.(2.13) is an orthogonal matrix which can be easily decoded using Alamouti code [25]. Using the received signal vector, the transmitted symbols can be easily detected by multiplying the received signal vector with the inverse of channel matrix. The Eq.(2.13) does not consider the full diversity capability of STBC.

In this research, a full diversity STBC will be considered where the received signal with noise $\mathbf{n}$ can be modeled as

$$\mathbf{y} = \mathbf{H}\mathbf{x} + \mathbf{n}. \tag{2.14}$$

The receive signal $\mathbf{y}$ is a vector defined as

$$\mathbf{y} = \begin{bmatrix} y_0^{(t)} \\ y_1^{(t)} \\ \vdots \\ y_0^{(t+3)} \\ y_1^{(t+3)} \\ y_0^{*(t+4)} \\ y_1^{*(t+4)} \\ \vdots \\ y_0^{*(t+7)} \\ y_1^{*(t+7)} \end{bmatrix}. \tag{2.15}$$

The entry of vector $\mathbf{y}$ is composed of received signal of each antenna for different time instances t to $(t+7)$.

In order to realize STBC process, a channel matrix $\mathbf{H}$ is used to multiply to the vector $\mathbf{y}$. The channel matrix $\mathbf{H}$ can be defined as

$$\mathbf{H} = \begin{bmatrix} \mathbf{J} \\ \mathbf{J}^* \end{bmatrix}, \tag{2.16}$$

where $\mathbf{J}$ is,

$$\mathbf{J} = \begin{bmatrix} h_{00} & h_{01} & h_{02} & h_{03} \\ h_{10} & h_{11} & h_{12} & h_{13} \\ h_{01} & -h_{00} & h_{03} & -h_{02} \\ h_{11} & -h_{10} & h_{13} & -h_{12} \\ h_{02} & -h_{03} & -h_{00} & h_{01} \\ h_{12} & -h_{13} & -h_{10} & h_{11} \\ h_{03} & h_{02} & -h_{01} & -h_{00} \\ h_{13} & h_{12} & -h_{11} & -h_{10} \end{bmatrix}. \tag{2.17}$$

Here we can observed that 4 symbols are transmitted at 2 time instances resulting to a STBC rate of 1/2.

With the STBC implementation in a single frequency network, it is expected that the diversity will increase if the receiver receives multiple signals from multiple transmitters. In [3], a diversity gain analysis using STBC-SFN was implemented using simulation. Figure 2.7 shows an illustration of coverage area of

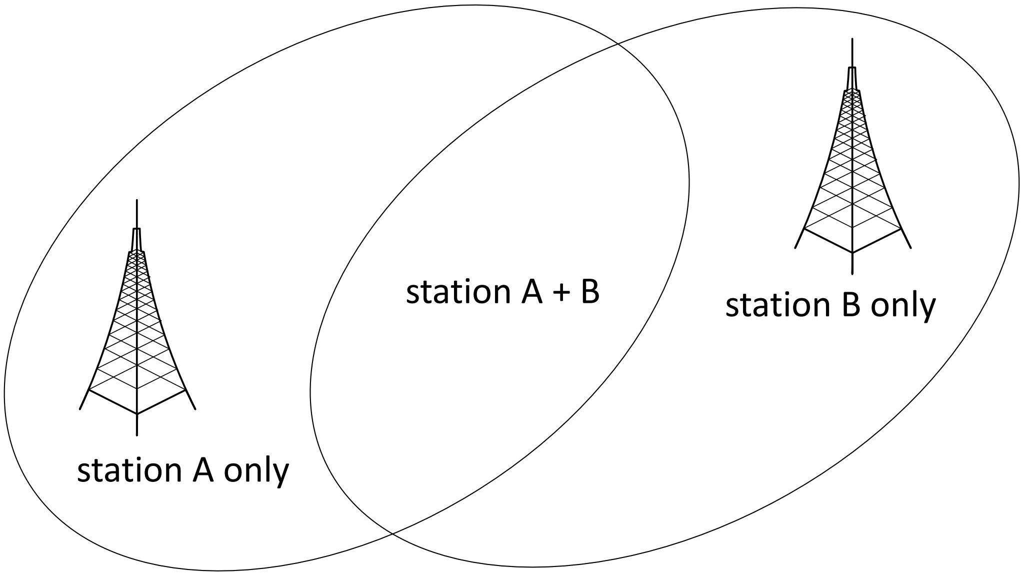

Figure 2.7: Coverage area of two transmitters (station A and station B) using Single Frequency Network

two transmitters where portion of the coverage area can receive signals from two transmitters (station A + B), while other coverage area can only receive signal from single transmitter (station A only or station B only).

Figure 2.8 shows the bit-error-rate (BER) performance comparison of the receiver placed in a station A + B coverage area and a receiver placed in station A only coverage area. A system with two receive signal from station A and B will have different receive signal power from different transmitters. Here we defined power difference (PD) as

$$\mathrm{PD} = 10 \cdot \log_{10} \frac{\text{receive signal power from station B}}{\text{receive signal power from station A}}. \tag{2.18}$$

We can observed in Fig.2.8 that the BER performance with two receive signal has less error compared to a receiver in station A only coverage area. In addition, we can also further reduce the error rate if the receiver receives higher power signal for both stations (PD=0dB) compared to negative value PD.

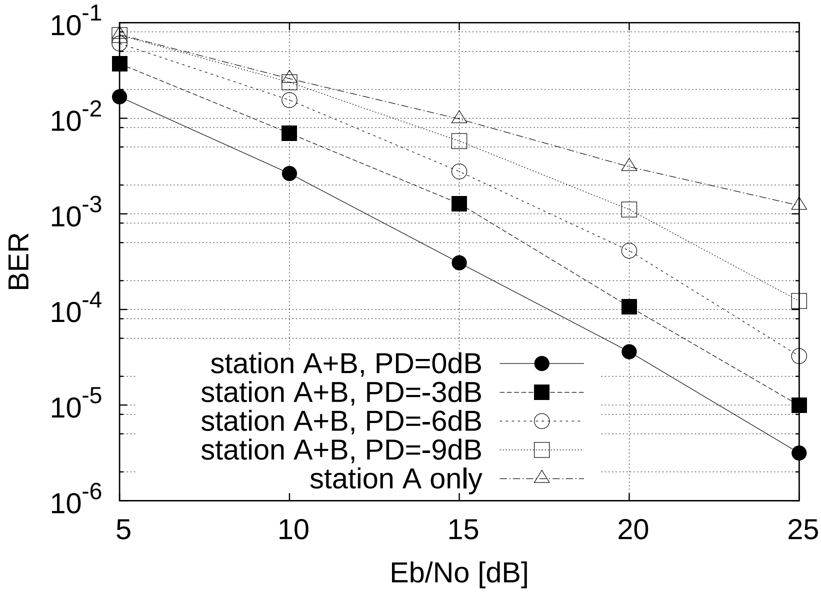

Figure 2.8: BER performance for two transmitters vs. one transmitter coverage areas

3 LDM for Migration of Next Generation DTTB System

The next generation generation DTTB systems such as 4K-resolution and 8K-resolution is currently on going development. While the ISDB-T that offers high definition TV (HDTV) [2] is currently used by people in Japan. The field experiment operated by Nippon Hoso Kyokai (NHK) successfully transmitted an 8K signal using STBC over a SFN system [22]. The experiment of the 8K DTTB system was conducted in a rural area so that TV subscribers will not be affected by co-channel interference. However, an issue needs to be considered is how to implement the next generation DTTB system without requiring new frequency resources. Currently, the UHF band from 470 MHz to 710 MHz are assigned for the ISDB-T [26]. One of the promising way is to transmit the next generation DTTB signal with the current ISDB-T signal over common frequency band simultaneously. In order to demodulate properly the ISDB-T stream, ISDB-T receiver will only require very simple STBC decoder. The contribution of this chapter can be defined below as:

1. The proposed system will have a very efficient spectrum resource utilization because of ISDB-T frequency spectrum reusing.

2. The primary layer is used not only for cancellation to obtained the secondary layer, but also part of the 4K UHD data. In this research, a combination of primary and secondary data stream is implemented to obtained a 4K UHD data.

3. With the reuse of primary layer to obtained the 4K data stream, we can reduce the capacity requirement of secondary data stream using partial

LDM. In that way, we can reduce the interference between primary and secondary layers of LDM.

3.1 Principle of LDM

In this research, the Layered Division Multiplexing (LDM) was implemented to exploit the non-orthogonal multiplexing capability of this technique [27]. LDM became popular for next generation DTTB because of its efficient frequency utilization and robust performance. In fact, the LDM was employed in ATSC 3.0 as a new technology for next generation DTTB system [10]. LDM is composed of two layers namely primary layer signal for high power signal transmission, and the secondary layer signal designed for high capacity transmission. The signal power of the secondary layer is very low wherein it is considered as an additional noise in reference to the high powered primary layer [28].

In the literature, there is a similarity between hierarchical modulation and LDM. But the next generation DTTB developers prefer to implement LDM compared to hierarchical modulation because LDM is more flexible. LDM has more freedom on how much transmission rate will be implemented for primary and secondary layer. It is because LDM uses two independent constellations with different transmission power overlapping with each other. While hierarchical modulation uses only single constellation for two different information (e.g. combination of 4-PSK for primary layer and 16QAM in the secondary layer results to a 64QAM) [29]. For 4-PSK in 64QAM hierarchical modulation, the number of bits per symbol in each subcarrier is 6, because 2 bits are modulated by using QPSK for primary layer, and additional of 4 bits are modulated for secondary layer. Another example is the QPSK/16QAM hierarchical modulation, where 4 bits per symbol are used [30]. In QPSK/16QAM hierarchical modulation, 2 bits are used for primary layer, while additional of 2 bits for the secondary data stream can be implemented. In summary, the conceptual difference between LDM and hierarchical modulation are: 1.) LDM is configured by use of spectrum overlap technology while the hierarchical modulation mainly focuses on backward compatibility and it does not based on spectrum overlapping. 2.) Hierarchical demodulator does not have signal cancellation capability compared to LDM. In

LDM, cancellation of multiple signals in different layers is necessity for demodulation.

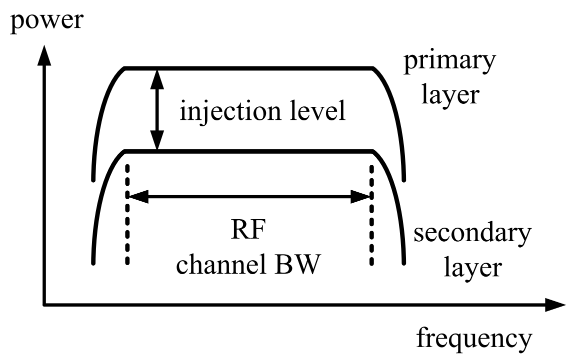

Figure 3.1: Bandwidth configuration using LDM for ISDB-T and secondary data stream

With the implementation of LDM as illustrated in Fig.3.1, a dual transmission of ISDB-T and secondary data stream is possible. In Fig.3.1, the primary layer is assigned for ISDB-T, and the secondary layer is assigned for secondary data stream. However, LDM is prone to interference due to superposition between the primary and secondary layer. And also, the primary layer symbol is wasted because it is only use for cancellation to obtain the secondary layer. In order to solve these issues, the proposed receiver reuses the primary layer to reconstruct higher data rate streams in combination with the secondary data stream. A related work is the augmented data transmission (ADT)-based ultrahigh definition (UHD) television transmission system using an existing ATSC terrestrial DTV system [31]. A combination of Moving Picture Experts Group-2 (MPEG-2) based DTV signal and High Efficiency Video Coding (HEVC)-based DTV signal to form a 4K UHDTV is implemented in ADT system.

A reduction of transmission capacity requirement for secondary data stream can be achieve because of reusing the ISDB-T data. With partial LDM implementation, we can reduce the interference between upper and lower layer. Hence, the secondary layer data stream does not lay down over the whole symbols, but partial secondary layer symbols are employed to transmit additional data. The ISDB-T data can be treated both as supplementary data for next generation DTTB system, and use in cancellation to obtain the secondary data stream.

3.2 Proposed LDM based system

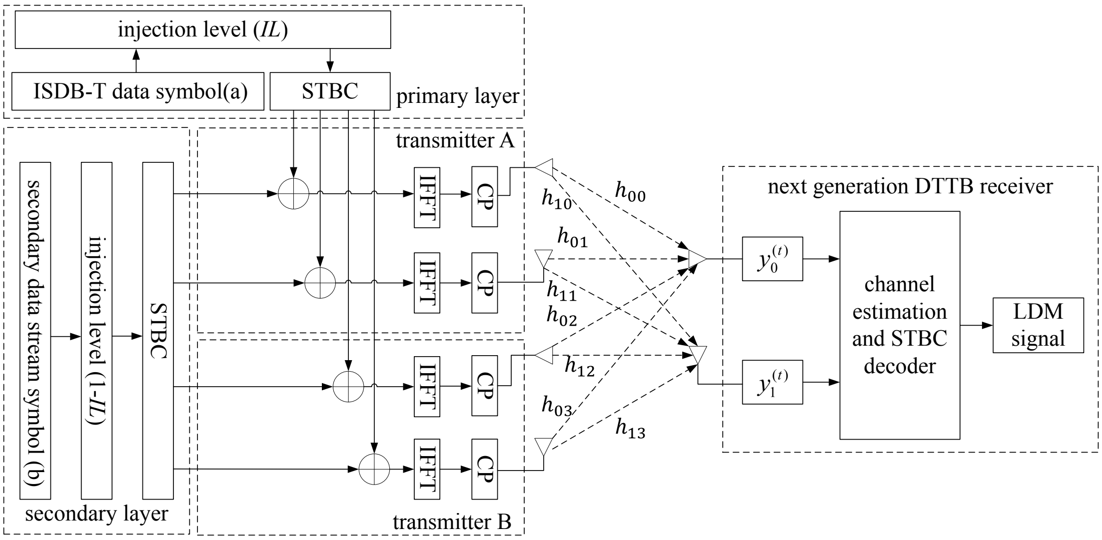

Figure 3.2: System block diagram of combined ISDB-T and next generation DTTB system using LDM

The SFN system block diagram using two transmitters and next generation DTTB receiver is shown in Fig.3.2. The next generation DTTB system adopts multiple transmitters that operates in an identical frequency band [23]. Each of the transmitters composes of two antennas with different polarities equivalent to a MIMO system. The dual polarized antennas transmit simultaneously using horizontal and vertical polarized waves for different data streams to increase of transmission capacity [22]. With the STBC-MIMO application, the diversity gain will increase and lessen the error-rate as shown in Fig.2.8 in the previous chapter.

A synchronization between different transmitters is necessary to avoid inter-symbol interference in SFN. One of the techniques for transmitters synchronization is longer duration cyclic prefix of OFDM systems. Longer duration CP makes the transmit delay among different transmitters fall within CP duration. Another promising technique is the STBC application. An Alamouti code is implemented in STBC to increase the MIMO diversity [25].

In the proposal, the ISDB-T is placed in the primary layer, while an additional data stream (HEVC) is used in the secondary layer. Combining both layers can achieve a 4K UHDTV signal. The ISDB-T data and secondary data stream are combined in frequency domain before IFFT. Before combining both layers, it is necessary to adjust the signal power for both layers using the injection level (IL).

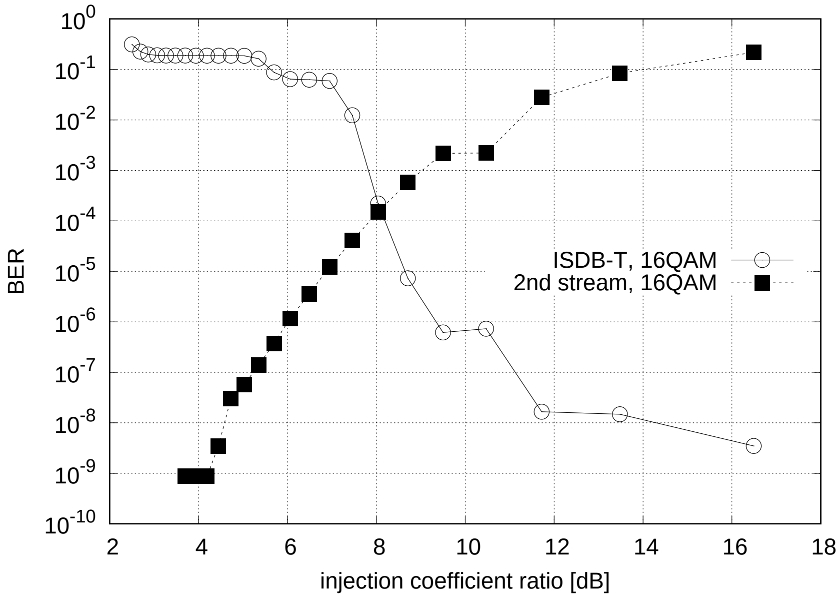

Figure 3.3: BER performance for different values of injection coefficient ratio

Figure 3.3 shows the method of choosing the optimum value of IL. Figure .3.3 shows the BER performance for the ISDB-T and secondary data stream with different values of injection coefficient ratio in the Eb/No=25dB. The injection coefficient ratio can be calculated by $10 \cdot \log(IL/(1-IL))$ [dB]. Higher injection coefficient ratio will increase the signal power of ISDB-T which result to a less error-rate for ISDB-T. On the other hand, lower injection coefficient ratio will increase the signal power of secondary data stream, which lessen the error-rate of secondary data stream. We can observe in the figure where the point of BER performance for both layers is almost identical is around 8dB. The optimum value of IL will depend on the modulation parameters of both LDM layers.

In Eq.(2.14), the transmitted signal $\mathbf{x}$ is composed of primary and secondary layer defined as

$$\mathbf{x} = \begin{bmatrix} IL \cdot a_0 + (1 - IL) \cdot b_0 \\ IL \cdot a_1 + (1 - IL) \cdot b_1 \\ IL \cdot a_2 + (1 - IL) \cdot b_2 \\ IL \cdot a_3 + (1 - IL) \cdot b_3 \end{bmatrix}, \tag{3.1}$$

where a_i and b_i corresponds to transmitting symbols for primary and secondary layer in the i-th symbol, respectively. Here we can observed that both ISDB-T signal and secondary data stream signal are both multiplied to the channel matrix $\mathbf{H}$ in Eq.(2.14) for STBC. This suggest that the ISDB-T signal also implements STBC process as shown in Fig.3.2.

In the proposal, a partial LDM assumed that the achievable capacity of the secondary layer exceeds the minimum requirements due to the reuse of the ISDB-T data as suggested in ADT system. The proof is provided in section 3.4. In that way, we need not to implement LDM for all the transmitted signal from ISDB-T transmission and next generation DTTB transmission. With the proposal of partial LDM, the Eq.(3.1) can be simplified into

$$\mathbf{x}_{(50)} = \begin{bmatrix} IL \cdot a_0 + (1 - IL) \cdot b_0 \\ IL \cdot a_1 + (1 - IL) \cdot b_1 \\ a_2 \\ a_3 \end{bmatrix}, \tag{3.2}$$

for 50% partial LDM where 2 out of 4 transmitted signals only implement LDM. On the other hand, the

$$\mathbf{x}_{(75)} = \begin{bmatrix} IL \cdot a_0 + (1 - IL) \cdot b_0 \\ IL \cdot a_1 + (1 - IL) \cdot b_1 \\ IL \cdot a_2 + (1 - IL) \cdot b_2 \\ a_3 \end{bmatrix}, \tag{3.3}$$

is for 75% partial LDM where 3 out of 4 transmitted signals are LDM implemented.

The pilots in ISDB-T are shared together with the secondary data stream system to avoid pilot interference between both layers. The scattered pilots (SP) are transmitted using

$$\begin{bmatrix} \mathrm{SP}_k \\ \mathrm{SP}_k \\ 0 \\ 0 \end{bmatrix}, \tag{3.4}$$

in the k-th subcarrier of transmitted signal $\mathbf{x}$. The SP subcarrier position is the same all throughout the transmitted signals. A detailed explanation about channel estimation in section 4.3 is provided on how to combined the different received pilots for interference avoidance.

3.3 Proposed LDM decoder

The LDM will allow two different signals to transmit using common frequency band. This suggests that LDM system will have two different receivers. This section will explain the details of two receivers: ISDB-T receiver with STBC decoder, and the next generation DTTB receiver for 4K UHDTV. The ISDB-T receiver with STBC decoder will demodulate the primary layer only. While the next generation DTTB receiver will demodulate the primary layer for initialization, and then a combination between both layers to obtain the 4K UHDTV signal.

3.3.1 Primary layer LDM decoder

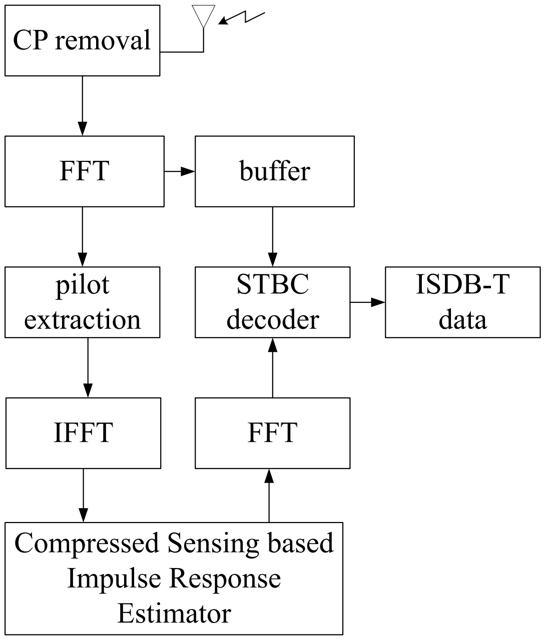

Figure 3.4: ISDB-T receiver with STBC decoder

The block diagram of the ISDB-T receiver is shown in Fig.3.4. The ISDB-T receiver is unconventional where an STBC decoder is needed to decode the ISDB-T signal. The received signal in Eq.(2.15) and the channel matrix in Eq.(2.16) are different for the case of ISDB-T because ISDB-T receiver is composed of single antenna only.

In the primary layer of LDM, the received signal for ISDB-T $\mathbf{y}_{(up)}$ is defined to be

$$\mathbf{y}_{(up)} = IL \cdot \mathbf{H}_{(up)}\mathbf{a} + (1 - IL) \cdot \mathbf{H}_{(up)}\mathbf{b} + \mathbf{n}_{(up)}, \tag{3.5}$$

where $\mathbf{a}^T = \begin{bmatrix} a_0 & a_1 & a_2 & a_3 \end{bmatrix}^T$ and $\mathbf{b}^T = \begin{bmatrix} b_0 & b_1 & b_2 & b_3 \end{bmatrix}^T$ are the transmitted ISDB-T data symbols and secondary data stream symbols, respectively. The entries of $\mathbf{y}_{(up)}$ are defined as,

$$\mathbf{y}_{(up)} = \begin{bmatrix} y_1^{(t)} \\ \vdots \\ y_1^{(t+3)} \\ y_1^{*(t+4)} \\ \vdots \\ y_1^{*(t+7)} \end{bmatrix}, \tag{3.6}$$

which are composed of symbols from received single antenna. While the channel matrix for ISDB-T $\mathbf{H}_{(up)}$ can be defined as

$$\mathbf{H}_{(up)} = \begin{bmatrix} h_{10} & h_{11} & h_{12} & h_{13} \\ h_{11} & -h_{10} & h_{13} & -h_{12} \\ h_{12} & -h_{13} & -h_{10} & h_{11} \\ h_{13} & h_{12} & -h_{11} & -h_{10} \\ h_{10}^* & h_{11}^* & h_{12}^* & h_{13}^* \\ h_{11}^* & -h_{10}^* & h_{13}^* & -h_{12}^* \\ h_{12}^* & -h_{13}^* & -h_{10}^* & h_{11}^* \\ h_{13}^* & h_{12}^* & -h_{11}^* & -h_{10}^* \end{bmatrix}. \tag{3.7}$$

In Eq.(3.5), we observe that the term $(1-IL)\cdot\mathbf{H}_{(up)}\mathbf{b}$ will add an interference to the ISDB-T received signal. To lessen the interference to the ISDB-T signal, the proposed system uses only partial LDM where only part of the total transmitted signal uses LDM [32]. In this way, we can minimize the value of $\mathbf{b}$ which results to a less interference to the received ISDB-T signal. The way the IL is chosen is describe in Fig.3.3, where the signal power of the secondary layer is reduced to lessen the interference with primary layer.

The estimated channel for ISDB-T $\hat{\mathbf{H}}_{(up)}$ can be obtain using CE in time domain with the help of the received pilot signals [18]. The CE is explain in section 4.3 where each entries of $\hat{\mathbf{H}}_{(up)}$ was obtained using CS based impulse response estimator. And then, the estimated channel for ISDB-T $\hat{\mathbf{H}}_{(up)}$ will be use to decode the ISDB-T symbols a_1, a_2, a_3, and a_4 using STBC [25] with the following equation

$$\hat{\mathbf{a}} = \frac{\hat{\mathbf{H}}_{(up)}^H}{\|\hat{\mathbf{H}}_{(up)}\|}\mathbf{y}_{(up)}, \tag{3.8}$$

where $\hat{\mathbf{a}}^T = \begin{bmatrix} \hat{a}_0 & \hat{a}_1 & \hat{a}_2 & \hat{a}_3 \end{bmatrix}^T$ is the estimated signals for ISDB-T. The notation $\|\cdot\|$ and $(\cdot)^H$ denote norm and Hermitian transpose, respectively. The STBC block in Fig. 3.4 is the equivalent of Eq.(3.8). Before performing the Eq.(3.8), the received signal is put in the buffer which is equivalent to $\mathbf{y}_{(up)}$.

3.3.2 Detection for secondary layer data stream

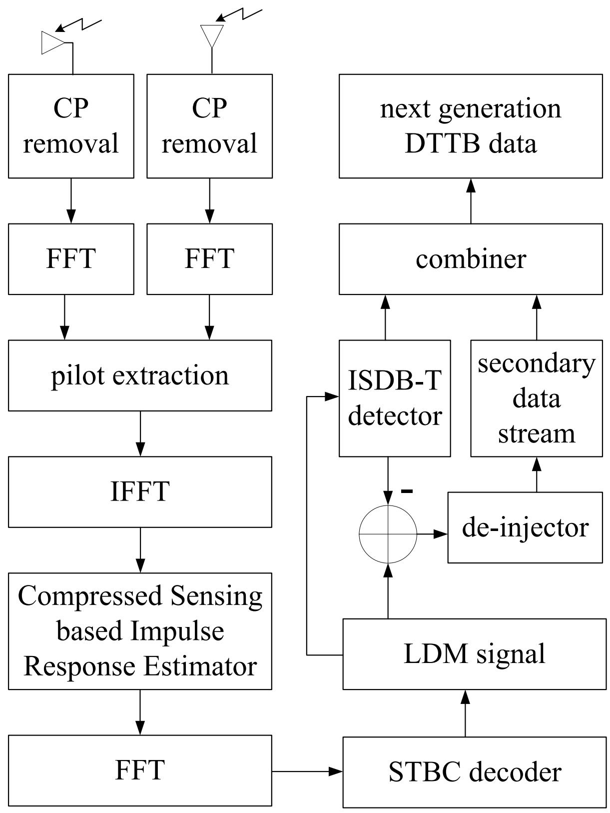

Figure 3.5: Proposed next generation DTTB receiver configuration using LDM

The previous section 3.3.1 explains the ISDB-T detection which is the first step for signal detection of the next generation DTTB receiver. The channel estimation is also using CS based impulse response estimator. The details about channel estimation is describe in section 4.2. The second step is the detection of the secondary data stream in the secondary layer. And finally, the last step is a combination of primary and secondary layer to obtain the 4K UHDTV signal.

The block diagram of the proposed next generation DTTB receiver is shown in Fig.3.5. The equivalent low pass received signal and channel response are denoted by $\mathbf{y}$ and $\mathbf{H}$, of Eq.(2.15) and Eq.(2.16), respectively. Here we can see that the receiver is composed of two antennas with different polarities while the ISDB-T receiver is only composed of single antenna.

Before detection of primary and secondary layer, a compressed sensing channel estimation is perform using the received pilot signals [18]. And then, diversity combined signal using STBC decoding can be determine using,

$$\hat{\mathbf{x}} = \frac{\hat{\mathbf{H}}^H}{\|\hat{\mathbf{H}}\|}\mathbf{y}, \tag{3.9}$$

where $\hat{\mathbf{x}}^T = \begin{bmatrix} \hat{x}_0 & \hat{x}_1 & \hat{x}_2 & \hat{x}_3 \end{bmatrix}^T$. From here we can detect the ISDB-T signal using exact the same procedure as describe in previous section 3.3.1. The second step is to estimate the secondary data stream $\hat{\mathbf{b}}$. Estimated symbol of secondary layer $\hat{\mathbf{b}}$ can be obtained as,

$$\hat{\mathbf{b}} = \frac{1}{1 - IL}(\hat{\mathbf{x}} - IL \cdot \hat{\mathbf{a}}). \tag{3.10}$$

Finally, we can exploit the ISDB-T data $\hat{\mathbf{a}}$ and the secondary data stream $\hat{\mathbf{b}}$ to acquire the whole transmitting data for 4K UHDTV using the combiner as described in Fig.3.5.

3.4 Achievable Channel Capacity

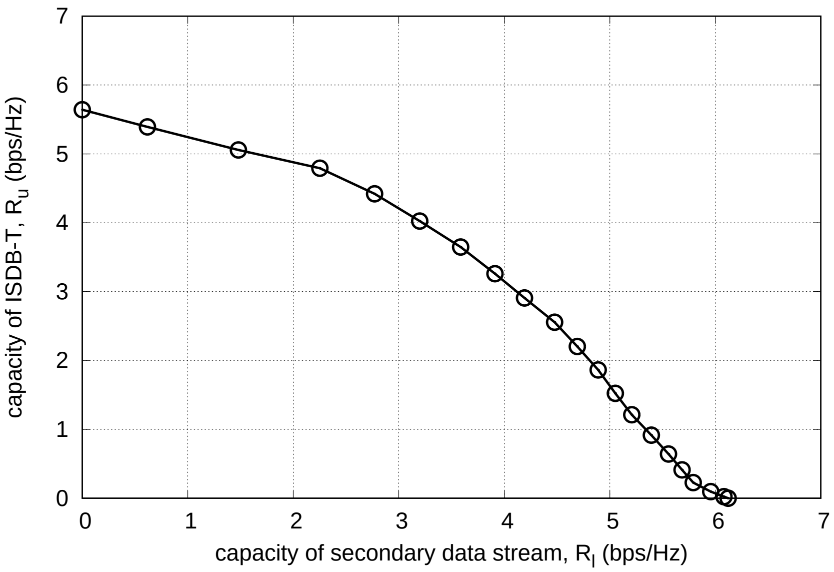

Figure 3.6: ISDB-T and secondary data stream capacity trade-off for LDM

The achievable channel capacity trade-off between ISDB-T and secondary data stream using LDM is shown in Fig.3.6. The channel capacity for the primary layer can be obtained using

$$R_u = R \cdot E\left[\log\left(1 + \sum_{n_m=0}^{7} \frac{IL^2 \frac{\mathrm{SNR}_u}{T_\mathrm{x}} ||[\mathbf{H}_{(up)}]_{n_m}||^2}{1 + (1-IL)^2 \frac{\mathrm{SNR}_u}{T_\mathrm{x}} ||[\mathbf{H}_{(up)}]_{n_m}||^2}\right)\right], \tag{3.11}$$

while the channel capacity for the secondary layer is

$$R_l = R \cdot E\left[\log\left(1 + (1-IL)^2 \frac{\mathrm{SNR}_l}{T_\mathrm{x}} ||\mathbf{H}||^2\right)\right]. \tag{3.12}$$

The above equations are related to the MIMO channel capacity of LDM [33] defined as

$$E\left[\log\det\left(\mathbf{I} + IL^2 \frac{\mathrm{SNR}_u}{T_\mathrm{x}} \mathbf{H}_{(up)}\mathbf{H}_{(up)}^H \cdot \left(\mathbf{I} + (1-IL)^2 \frac{\mathrm{SNR}_u}{T_\mathrm{x}} \mathbf{H}_{(up)}\mathbf{H}_{(up)}^H\right)^{-1}\right)\right], \tag{3.13}$$

for the upper layer, and

$$E\left[\log\det\left(\mathbf{I} + (1-IL)^2 \frac{\mathrm{SNR}_l}{T_\mathrm{x}} \mathbf{H}\mathbf{H}^H\right)\right] \tag{3.14}$$

for the lower layer. The STBC achievable capacity is lesser compared to MIMO channel capacity because STBC transmits repeated symbols. However, the error-rate for STBC is less which is ideal for higher modulation type such as 64QAM, 256QAM, etc.

For the derivation of Eq.(3.11), Let us first define a ergodic spectral efficiency of STBC as [33]

$$R \cdot E\Bigg[\log(1+\mathrm{SNR})\Bigg],$$

where the STBC maximal rate R

$$R = \frac{T_{\mathrm{x}}/2+1}{T_{\mathrm{x}}},$$

for T_{x} even, and

$$R = \frac{(T_{\mathrm{x}}+1)/2+1}{T_{\mathrm{x}}+1},$$

for T_{x} odd.

For simplicity, let us assumed that $T_{\mathrm{x}} = 2$. The Alamouti scheme operates across two successive channels i.e. subcarriers $j = 1, 2$. The received signal for the primary layer can be described as

$$\mathbf{y}_{(up)}[j] = IL\sqrt{\mathrm{SNR}_u}\mathbf{H}_{(up)}\mathbf{a}[j] + (1-IL)\sqrt{\mathrm{SNR}_u}\mathbf{H}_{(up)}\mathbf{b}[j] + \mathbf{n}[j].$$

The $\mathbf{b}[j]$ can be treated as Gaussian noise with zero mean, covariance matrix $\mathbf{I}/2$ where $1/2$ accounts for the power allocation of 2 antennas. As a result, the effective noise $\mathbf{n}_{\mathrm{eff}}[j] = (1-IL)\sqrt{\mathrm{SNR}_u}\mathbf{H}_{(up)}\mathbf{b}[j] + \mathbf{n}[j]$.

For each received signal, the effective noise power can be approximated to be $1 + (1-IL)^2\mathrm{SNR}_u||[\mathbf{H}_{(up)}]_{n_m}||^2/2$, where $[\mathbf{H}_{(up)}]_{n_m}$ is the n_m-th row of $\mathbf{H}_{(up)}$.

For example, in the case of two channels e.g. $j = 1, 2$, the received signal can be written as

$$\begin{bmatrix} \Big[\mathbf{y}_{(up)}[1]\Big]_{n_m} \\ \Big[\mathbf{y}_{(up)}[2]\Big]^*_{n_m} \end{bmatrix} = IL\sqrt{\mathrm{SNR}_u} \begin{bmatrix} \Big[\mathbf{H}_{(up)}\Big]_{n_m,1} & \Big[\mathbf{H}_{(up)}\Big]_{n_m,2} \\ \Big[\mathbf{H}_{(up)}\Big]^*_{n_m,2} & -\Big[\mathbf{H}_{(up)}\Big]^*_{n_m,1} \end{bmatrix} \cdot \begin{bmatrix} u_1 \\ u_2 \end{bmatrix} + \begin{bmatrix} [\mathbf{n}_{\mathrm{eff}}[1]]_{n_m} \\ [\mathbf{n}_{\mathrm{eff}}[2]]_{n_m} \end{bmatrix}$$

where $\begin{bmatrix} u_1 & u_2 \end{bmatrix}^T$ is the transmitted information symbols with power $1/2$. And then, projecting the transmitted vector into k-th column of the channel matrix will result to a signal equal to

$$IL\sqrt{\mathrm{SNR}_u}||[\mathbf{H}_{(up)}]_{n_m}||^2 u_k + w_k$$

Table 3.1: Calculation parameters for capacity trade-off of LDM

STBC rate (R)	3/4
number of transmitter antenna (T_{x})	4
primary layer threshold (SNR_u)	20 dB
secondary layer threshold (SNR_l)	25 dB
primary layer channel matrix ($\mathbf{H}_{(up)}$)	Eq. 3.7
secondary layer channel matrix ($\mathbf{H}$)	Eq. 2.16
injection level (IL)	$0 \sim 1$

where noise w_k has a power equivalent to $1 + (1 - IL)^2 \mathrm{SNR}_u ||[\mathbf{H}_{(up)}]_{n_m}||^2/2$. Finally, the SNR can be calculated as

$$\mathrm{SNR} = \frac{IL^2 \cdot \mathrm{SNR}_u ||[\mathbf{H}_{(up)}]_{n_m}||^2}{2(1 + (1 - IL)^2 \cdot \mathrm{SNR}_u ||[\mathbf{H}_{(up)}]_{n_m}||^2/2)}.$$

Table 3.1 shows the calculation parameters used for LDM capacity trade-off. The R and T_{x} are the STBC maximal rate and number of transmitter antennas, respectively [33]. While the SNR_u and SNR_l refers to the SNR threshold for primary and secondary layer, respectively. Because both ISDB-T receiver and 4K receiver are using roof-top antennas, we assume that the value of $\mathrm{SNR}_u = 20$dB, and $\mathrm{SNR}_l = 25$dB which is a reasonable value for this type of antenna [27].

The required bit-rate for ISDB-T is 3bps/Hz for a 6MHz bandwidth. Based on Fig.3.6, the achievable spectral efficiency for secondary data stream will be around 24Mbps given a 3bps/Hz for ISDB-T. A 24Mbps channel capacity is assumed to have an ideal channel coding, and a perfect channel estimation wherein pilots are unnecessary. We also assumed that the receiver side uses a maximum ratio combiner for the received signals. A 24Mbps for secondary data stream is too high since the requirement is only around 12.5Mbps. With the reuse of the ISDB-T data for next generation DTTB system, we can reduce the capacity load for the secondary data stream. Because of this reason, we propose a partial LDM to reduce the capacity of the secondary layer at least 12.5Mbps based on ADT system. In this way, we can reduce the interference for both layers of LDM using the proposed method.

3.5 Comparison between HEVC and MPEG-2

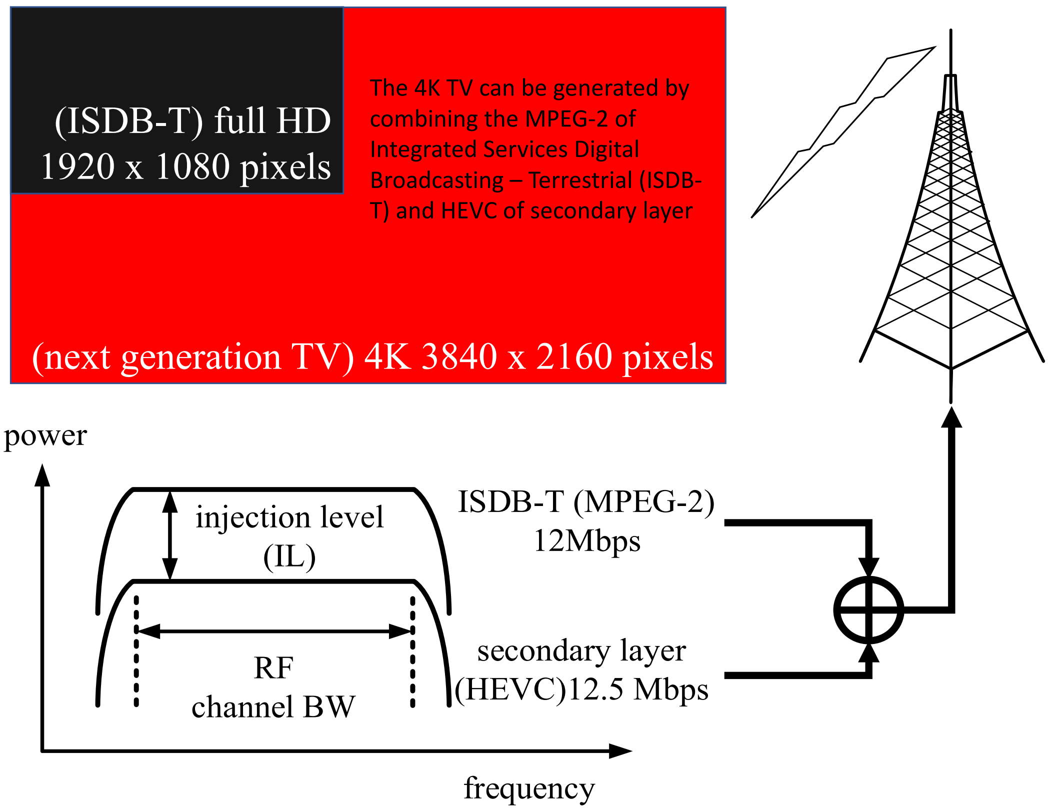

Figure 3.7: Combination of MPEG-2 of ISDB-T and HEVC of secondary data stream using LDM

For the DTTB system using ADT as shown in Fig.3.7, the capacity will only require 12Mbps for MPEG-2 signal, and 12.5Mbps for HEVC signal to form a 4K (30 frames) UHDTV [31]. The HEVC is an emerging video coding technology that provides around 65% bit-rate savings for equivalent perceptual quality relative to MPEG-2 standard [34]. In [4], the HEVC was compared with different video coding technologies in terms of bit-rate saving and peak signal to noise ratio on reversible luminance and chrominance (YUV-PSNR). The YUV-PSNR is defined as

$$\text{YUV-PSNR} = 10 \cdot \log_{10}\left(\frac{\text{MAX}^2}{\frac{1}{mn}\sum_{i=0}^{m-1}\sum_{j=0}^{n-1}\Big[I(i,j) - K(i,j)\Big]^2}\right)[\text{dB}], \tag{3.15}$$

where MAX is the maximum possible pixel value of the picture, and the denominator represents as mean squared error of noise-less m x n image I and estimated image K. The higher the YUV-PSNR indicates high quality image reconstruction.

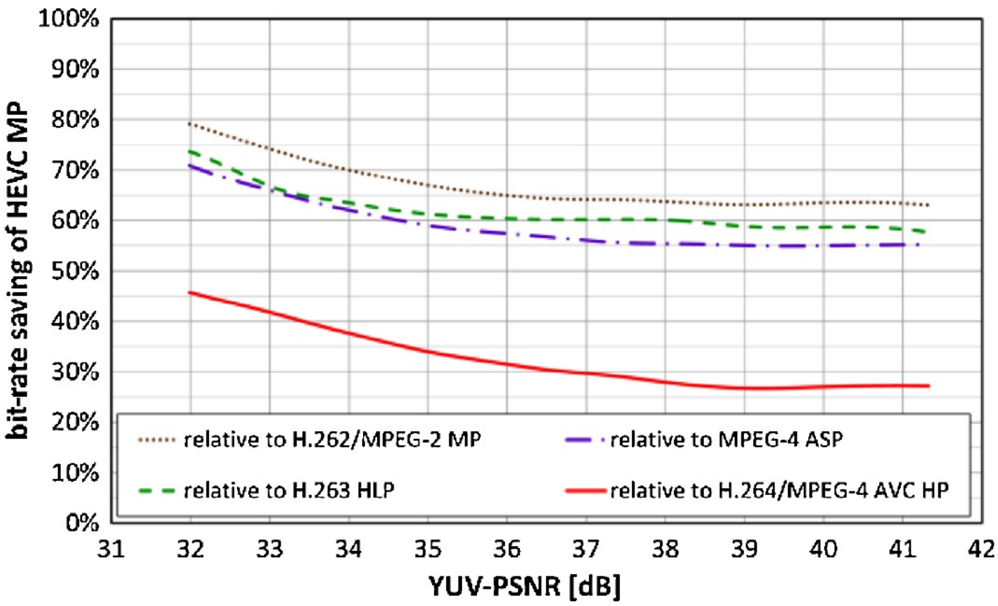

Figure 3.8: bit-rate saving of HEVC (Main Profile) MP relative to other video coding techniques [4]

Figure 3.8 shows the bit-rate saving of HEVC MP in relative to other video coding techniques. For the case of MPEG-2 MP for ISDB-T, around 65% bit-rate saving can be achieve using HEVC with the same video quality of MPEG-2 in higher YUV-PSNR region. In addition, the Fig.3.9 shows the YUV-PSNR for different video coding standards in terms of bit-rate. Higher bit-rate for each standard will increase the video quality as observed in increasing YUV-PSNR of the figure. For the requirement around 12Mbps region, we can observed that around 3dB YUV-PSNR improvement can be realized using HEVC in relative to MPEG-2 for ISDB-T. Without any doubt, a 4K TV service can be realize by combining MPEG-2 with HEVC using LDM.

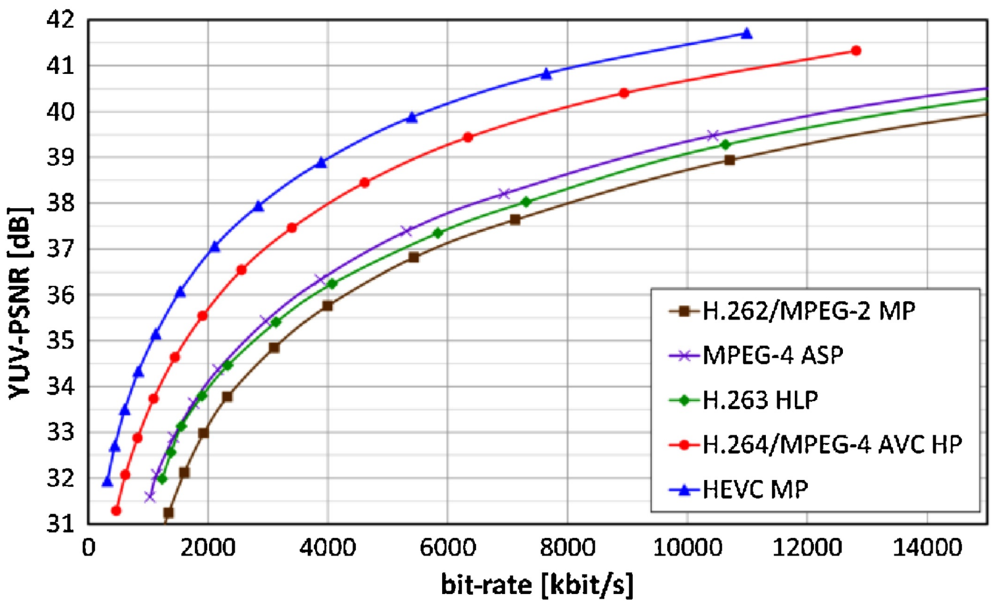

Figure 3.9: YUV-PSNR vs. bit-rate for different video coding standards [4]

3.6 Numerical Analysis

Table 3.2: Simulation parameters for the proposed LDM system

LDM layer	primary	secondary
data	ISDB-T	secondary data stream
modulation	QPSK, 16QAM	QPSK, 16QAM, 64QAM 256QAM
channel estimation (CE)	OMP	OMP with perfect ISDB-T detector
OMP iteration (η)	6	6
injection coefficient ratio $10 \cdot \log(IL/(1-IL))$	fig.3.10→ 12dB fig.3.11 → 10.6dB 16QAM in fig.3.13,3.15,3.16 → 8dB 64QAM in fig.3.16 → 7.5dB 256QAM in fig.3.16 → 6.9dB QPSK in fig.3.12,3.14 → 6dB	
FFT size (N)	8192	
number of pilot (M)	1024	
pilot type	scattered	
guard interval	$N/16$	
OFDM frame	10,000	
channel model	TU6	
noise type	AWGN	

A C++ library for signal processing and communication was used for computer simulation to analyze the performance of the proposed system [35]. Table 3.2 shows the simulation parameters of the experiment for both primary and secondary layers of LDM. For simplicity purposes, a forward error correction for primary layer is assumed to be ideal e.g. perfect ISDB-T detector. Table 3.3 shows the delay profile of the TU6 channel model used in the simulation [36]. In this simulation, the performance of the ISDB-T system for primary layer, and the secondary layer are investigated separately. The Eb/No that was used in this

Table 3.3: TU6 delay profile

delay (μs)	power (dB)
0	-3
0.2	0
0.5	-2
1.6	-6
2.3	-8
5.0	-10

experiment is the Eb/No of the secondary layer as a reference.

The first part of the experiment covers the bit-rate analysis for both LDM layers. Then, the BER performance of the conventional ISDB-T receiver without STBC decoder will be evaluated. After that, the BER performance for single transmitter vs. multiple transmitter will be analyzed. The last part of the experiment will discuss the performance of the proposed partial LDM.

3.6.1 Bit-rate performance for the different layers of LDM

Table 3.4: bit rate of full LDM and partial LDM in different modulation type

modulation type	full LDM	75% LDM	50% LDM
QPSK	7.11Mbps	5.33Mbps	3.56Mbps
16QAM	14.22Mbps	10.67Mbps	7.11Mbps
64QAM	21.33Mbps	16.00Mbps	10.67Mbps
256QAM	28.44Mbps	21.33Mbps	14.22Mbps
1024QAM	35.56Mbps	26.67Mbps	17.78Mbps

The bit rate for different modulation type vs. LDM type is shown in table 3.4. The bit rate is calculated using

$$\frac{(\text{STBC rate}) \cdot (N - M) \cdot \log_2(\text{modulation type})}{\text{OFDM effective symbol period}},$$

where the STBC rate are 1/2, 3/8, and 1/4 for full LDM, 75% LDM, and 50% LDM, respectively. The OFDM effective symbol period is 1008μs [2]. The bit rate shown in the table is both applicable for primary and secondary layer since both layer exhibit STBC transmission. The bit-rate shown in the table does not consider the condition of the wireless channel. The consideration of wireless channel will be included in BER performance in the succeeding subsection of numerical analysis.

3.6.2 BER performance using conventional ISDB-T receiver without STBC decoder

In this section, performance evaluation of the system using the conventional ISDB-T receiver without STBC decoder will be evaluated. The details about conventional ISDB-T receiver was also discussed in details in the previous section 2.1.1. The conventional ISDB-T receiver can demodulate without any problem using

$$\begin{bmatrix} IL \cdot a + (1 - IL) \cdot b_0 \\ IL \cdot a + (1 - IL) \cdot b_1 \\ (1 - IL) \cdot b_2 \\ (1 - IL) \cdot b_3 \end{bmatrix}, \tag{3.16}$$

as a transmitted signal for Eq.(3.1). For simplicity purposes, we use the same ISDB-T symbol a for all time instances t to $t + 7$. The way the detection of conventional ISDB-T receiver is for every time instance. For example in time instance t at the received signal $y_1^{(t)}$, the received signal will be

$$\begin{aligned} y_1^{(t)} =& IL \cdot a \cdot h_{10} + (1 - IL) \cdot b_0 \cdot h_{10} + IL \cdot a \cdot h_{11} + \\ & (1 - IL) \cdot b_1 \cdot h_{11} + (1 - IL) \cdot b_2 \cdot h_{12} + \\ & (1 - IL) \cdot b_3 \cdot h_{13} + n \end{aligned}$$

The effective noise n_{eff} will be

$$\begin{aligned} n_{eff} =& (1 - IL) \cdot b_0 \cdot h_{10} + (1 - IL) \cdot b_1 \cdot h_{11} + \\ & (1 - IL) \cdot b_2 \cdot h_{12} + (1 - IL) \cdot b_3 \cdot h_{13} + n. \end{aligned}$$

The received signal can now be simplified as

$$y_1^{(t)} = IL \cdot a \cdot (h_{10} + h_{11}) + n_{eff}.$$

Here we can measure the channel $(h_{10} + h_{11})$ because a contains the pilots based on eq. 3.4. Dividing the whole equation above with $(h_{10} + h_{11})$ will result to a detection of $\tilde{a}$

$$\tilde{a} = \frac{y_1^{(t)}}{(h_{10} + h_{11})} = IL \cdot a \cdot + \frac{n_{eff}}{(h_{10} + h_{11})}.$$

The value of IL should be high enough for decent detection of a. The process above is also the same in other receive signals $y_1^{(t+1)}, ..., y_1^{(t+7)}$.

The BER performance for the conventional ISDB-T, and the secondary data stream for next generation DTTB receiver is shown in Fig. 3.10. Both layers are using QPSK in this simulation. From the shown figure, we observed that the ISDB-T receiver has low error rate compared to that of secondary data stream because primary layer has higher power compared to the secondary layer. The BER performance for ISDB-T is within acceptable error rate in the Eb/No=25dB region using QPSK for both layers. However, the performance for the secondary data stream is only limited to the low order modulation such as QPSK. Because of this reason, it is necessary to implement an STBC decoder for ISDB-T receiver to drastically reduce the error rate and provides an opportunity to implement higher order modulation for the secondary data stream.

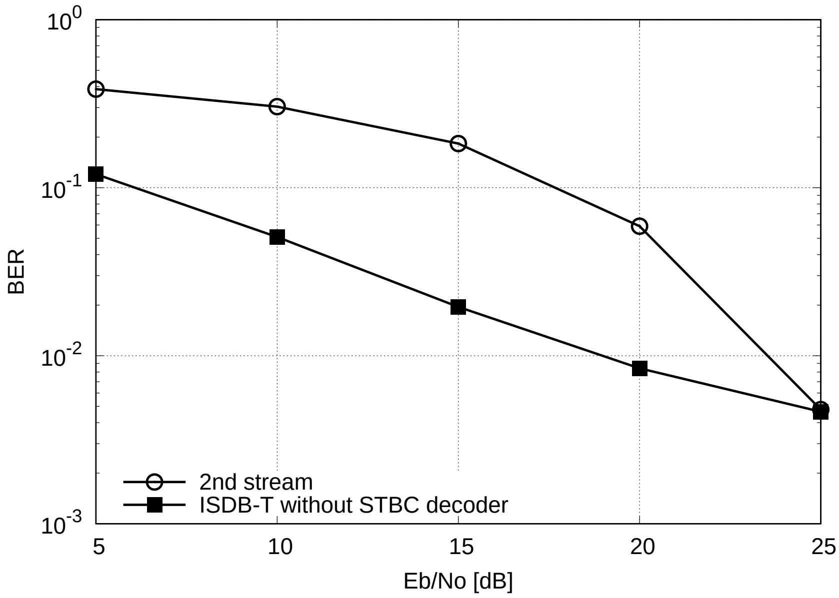

Figure 3.10: BER performance using conventional ISDB-T receiver without STBC decoder (QPSK), and the secondary data stream (QPSK)

To fully qualify for 4K UHDTV transmission, the secondary layer should use at least 16QAM so that the bit-rate will be 14.22Mbps based on table 3.4 which is above the required 12.5Mbps. While the bit-rate of the primary layer will also equal to 14.22Mbps even though we are only using QPSK because STBC rate is equal to 1 for conventional ISDB-T receiver without STBC decoder. Figure 3.11 shows the BER performance where the secondary layer is using 16QAM. We also observe that there is a little performance degradation in the Eb/No=25dB compared to Fig.3.10. That is because the secondary layer is now using 16QAM modulation type. Nevertheless the BER performance in Eb/No=25dB is still within 10^{-3} to 10^{-2}.

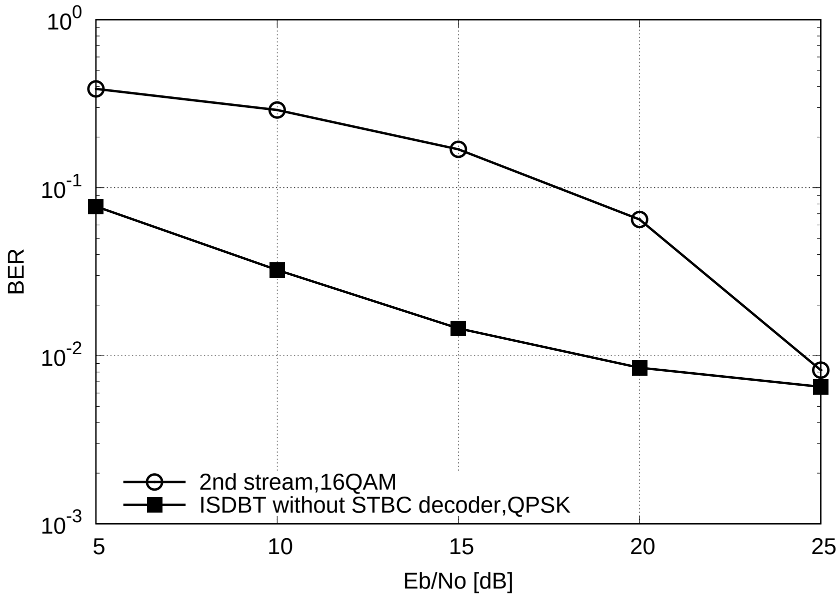

Figure 3.11: BER performance using conventional ISDB-T receiver without STBC decoder (QPSK), and the secondary data stream (16QAM)

3.6.3 Diversity gain analysis using multiple transmitters

In the previous section 2.2.1, the diversity gain of STBC-SFN was discussed where the multiple transmitters has higher diversity with less error-rate compared to a system with only single transmitter. In this section, we evaluate the diversity gain of STBC-SFN with LDM. Here we implement ISDB-T receiver with STBC decoder to improve the diversity and lessen the error rate.

The simulation compares the BER performance of two transmitters and single transmitter as discussed in Fig.2.7 of section 2.2.1. The pairs in the simulations (e.g. pair A, pair B, and pair C) indicate the pair of primary and secondary layers of LDM. For example in Fig.3.12, pair A describes the ISDB-T as a primary layer, and 2nd stream as a secondary layer wherein the system has 2 transmitters. On the other hand, the pair B indicates that the primary layer is the ISDB-T, and the secondary layer is the 2nd stream where the system only uses 1 transmitter.

The BER performance of the ISDB-T receiver and secondary data stream using QPSK is shown in Fig.3.12. In Fig.3.12, we compare the performance with two transmitters versus single transmitter using full LDM. In order to realize single transmitter, the values of $h_{02}, h_{12}, h_{03}, h_{13}$ of $\mathbf{J}$ and $\mathbf{H}_{(up)}$ will be set to zero. The $h_{02}, h_{12}, h_{03}, h_{13}$ are the channels for transmitter B in Fig.3.2. While for the case of two transmitter, the values of $h_{02}, h_{12}, h_{03}, h_{13}$ of $\mathbf{J}$ and $\mathbf{H}_{(up)}$ will be nonzero. In Fig.3.12, the error rate for 2 transmitters is less compared to single transmitter. It is found that the diversity improves the performance when the number of transmitter increases. In the Eb/No region of 25dB, we can improve up to 10dB for ISDB-T, while 5dB for secondary data stream. This suggest that increasing the number of transmitters will increase the diversity of the whole system.

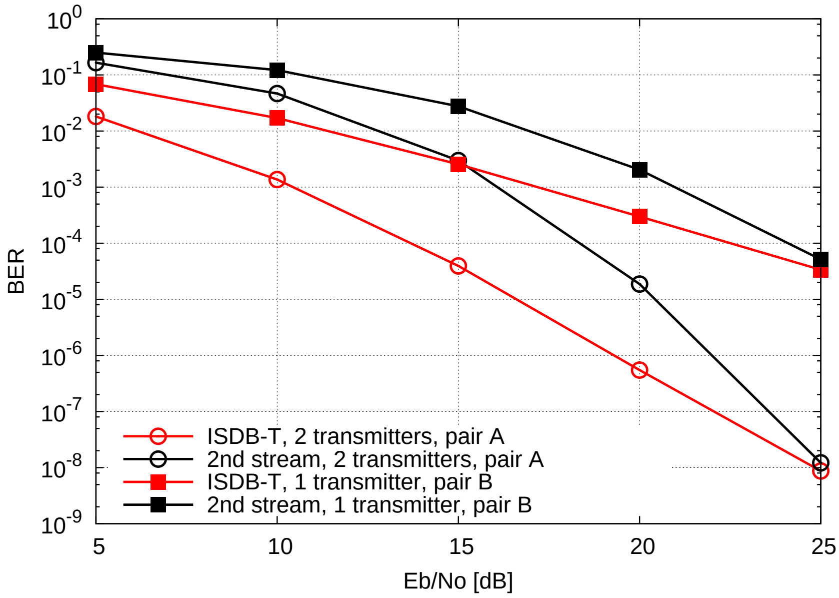

Figure 3.12: BER performance for 2 transmitters vs. 1 transmitter using QPSK full LDM

Similarly, the BER performance of 16QAM for both LDM layers is shown in Fig.3.13. In this figure, the performance for 2 transmitters has less error rate compared with single transmitter. In Eb/No region of 25dB, the diversity improves the performance of both layers by around 5dB. This kind of BER performance can also observed in Fig.2.8 of the previous section 2.2.1.

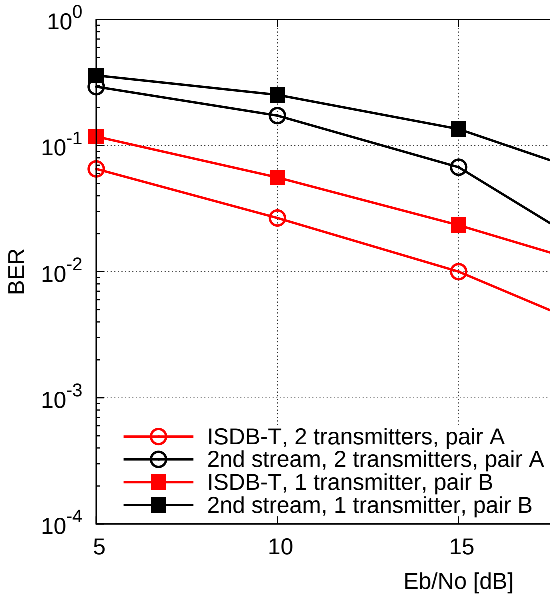

Figure 3.13: BER performance for 2 transmitter vs. 1 transmitter using 16QAM full LDM

3.6.4 BER performance of partial LDM

The BER performance of partial LDM using QPSK for both LDM layers is shown in Fig.3.14. In this figure, we compare partial LDM of 50%, partial LDM of 75%, and the full LDM. The transmitted signal for partial LDM of 50% and 75% can be described in Eq.(3.2) and Eq.(3.3), respectively. Here we observed that the secondary data stream performance is the same in spite of partial use in LDM. The partial LDM slightly changes the ISDB-T BER performance. In Fig.3.14, we observed a higher error rate in case of ISDB-T full LDM compared to ISDB-T partial LDM. Because the modulation for both layers is only QPSK, the improvement of ISDB-T partial LDM is only 1dB in reference to ISDB-T full LDM.

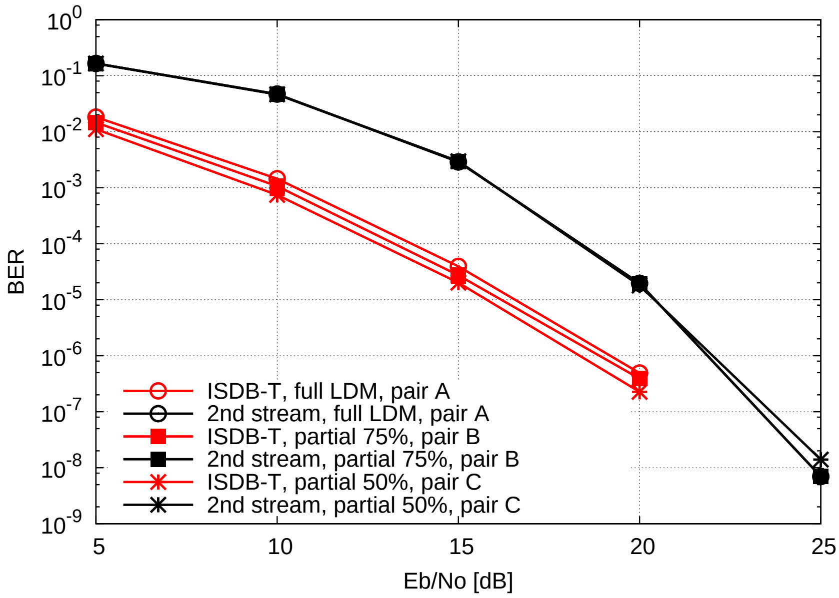

Figure 3.14: BER performance for full LDM vs. partial LDM using QPSK

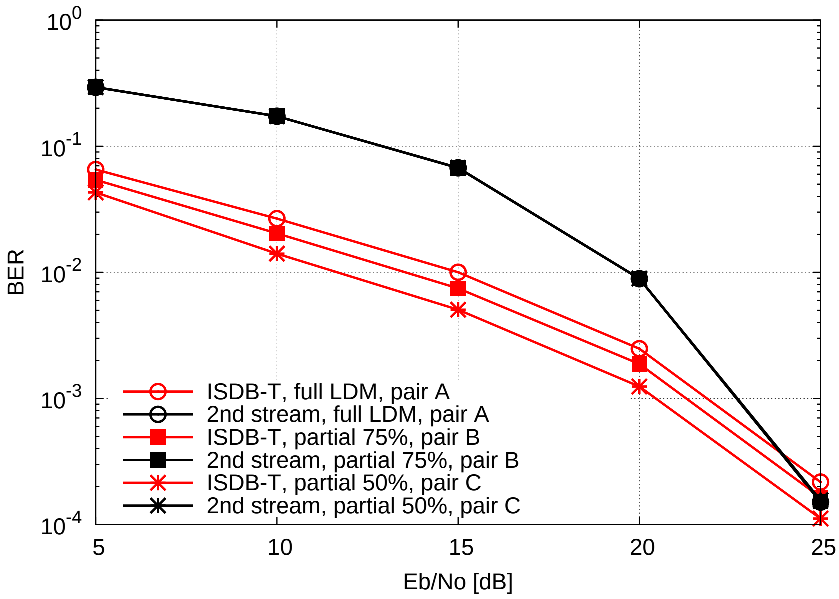

Figure 3.15: BER performance for full LDM vs. partial LDM using 16QAM

However for the case of 16QAM for both LDM layers as shown in Fig.3.15, we observed that the error rate for the ISDB-T partial LDM of 50% and 75%

has a respective improvement around 2dB and 1dB lower compared to full LDM in the Eb/No region of 25dB. The reason why partial LDM has lesser error-rate compared to full LDM because the term $(IL \cdot \mathbf{H}_{(up)}\mathbf{b})$ in Eq. (3.5) is less because of less non-zero entries of vector $\mathbf{b}$. In the end, there will be less interference between both LDM layers.

The bit-rate requirement for 4K UHDTV using LDM is at least 12Mbps for primary layer and 12.5Mbps for secondary layer based on ADT system [31]. Based on table 3.4, the primary layer and secondary layer can use 16QAM or higher order using full LDM. In Fig. 3.15, the full LDM for both layers using 16QAM qualifies to transmit a 4K transmission. Other option is using a 16QAM for primary layer, and 64QAM in the secondary layer. However, the transmission capacity using 64QAM full LDM is around 21.33Mbps which is high enough in comparison to a minimum requirement of 12.5Mbps. In that way, a 75% partial LDM can be applied to reduce the transmission capacity to 16Mbps and lessen the bit error rate in the primary layer. Figure 3.16 shows the other BER performance of the primary layer set to 16QAM, together with various modulation type in the secondary layer. All the parameters in Fig.3.16 is capable of 4K transmission. In this figure, the Eb/No is set to 25dB. Here we can observe that we can gradually reduce the error for the primary layer using partial LDM especially for higher modulation type such as 64 QAM and 256 QAM. This suggest that partial LDM is very applicable for higher modulation type.

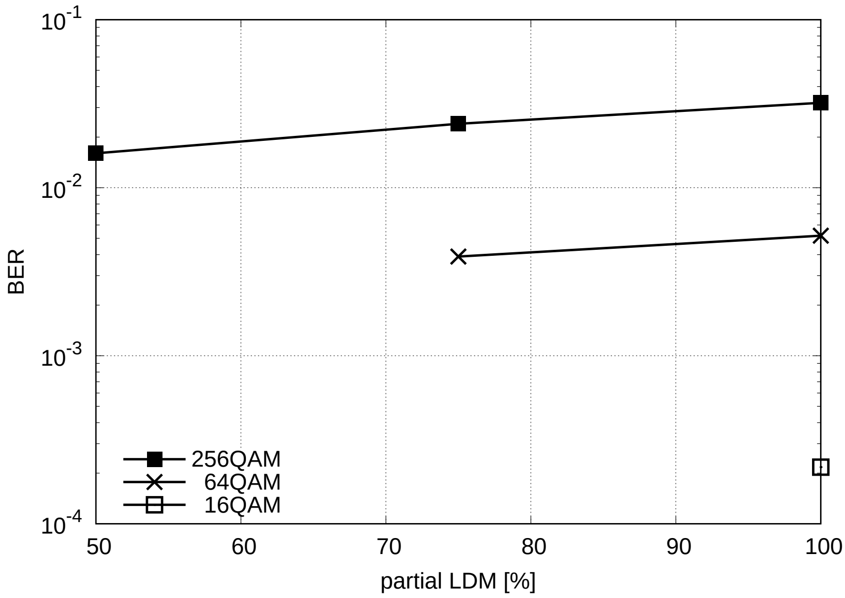

Figure 3.16: BER performance for primary layer using various modulation type in secondary layer; Eb/No=25dB, 16QAM for primary layer

To summarize the simulation results in this section, the BER performance for ISDB-T without STBC decoder is within acceptable level. However, the modulation type for secondary layer is only limited to low order type, e.g. QPSK, 16QAM. With the ISDB-T receiver with STBC decoder, it can lessen the error rate which opens an opportunity for the secondary layer to implement higher order modulation. Increasing the number of transmitters can also lessen the error rate for both primary and secondary layer due to STBC diversity. In addition, implementing a partial LDM can lessen further the error rate due to less interference between primary and secondary layer. The higher the modulation type being used, the lower the interference between LDM layers uing the proposed partial LDM.

3.7 Summary

This chapter proposed an efficient broadcast transmission system for the ISDB-T system and next generation terrestrial DTTB system using the identical frequency spectrum. For efficient frequency spectrum utilization, we implemented LDM to transmit the ISDB-T in the primary layer and a secondary data stream in the secondary layer of LDM. To increase the diversity gain, the proposed system is using space time block coding in a single frequency network.

The next generation DTTB system reuses the primary layer by combining the ISDB-T data and the secondary data stream. With this idea, the ISDB-T data will not be wasted because the ISDB-T is reused to construct the 4K TV signal. In addition, we can lessen the interference between two LDM layers by implementing partial LDM where only few transmitted signal uses LDM. Partial LDM can be applied since the achievable capacity for the secondary layer exceeds the required capacity of 12.5 Mbps. The proposed system should have at least 12Mbps in the primary layer and 12.5Mbps in the secondary layer to achieve a 4K UHDTV transmission.

The proposed system is applicable for conventional ISDB-T receiver without STBC decoder. However, the simulation of the conventional ISDB-T without STBC decoder shows an acceptable error rate of 10^{-3} to 10^{-2} in the Eb/No=25dB region. And also, the modulation type for the secondary layer is only limited to lower modulation type (QPSK or 16QAM). This suggest an implementation of STBC decoder for ISDB-T to increase the diversity. The simulation for LDM-STBC with multiple transmitters shows that error rate for both layers can be lessen compared to the system with only single transmitter.

In addition, the BER performance of primary layer was further improved by introducing partial LDM. To fully qualify for 4K transmission, both layers should be at least 16QAM. Other option is to implement partial LDM in the secondary layer using modulation type higher than 16QAM as long as the bit-rate for primary and secondary layer is 12Mbps, and 12.5Mbps, respectively.

4 Time Domain Compressed Sensing based Channel Estimation for DTTB System

This chapter will discuss about the channel estimation (CE) used in ISDB-T receiver and proposed next generation DTTB receiver. CE is usually performed using pilots that are inserted in some OFDM subcarriers [37]. The pilots will serve as a training method for CE. Using the received pilots, the receiver can estimate the channel frequency response (CFR) based on particular criterion such as, Least Square (LS) or Minimum Mean Square Error (MMSE) [38]. CE can be erroneous due to the thermal noise in the receiver circuit.

In this research, time domain CE has been considered to exploit the sparse feature of CIR [39]. Because of the fact that CIR is always zero beyond the guard interval of OFDM symbol, time domain CE algorithms estimate only CIR within the guard interval for complexity reduction. For the DTTB system, the CIR is always sparse where there are only few paths having dominant power, thus, CS-based CE can be applied for further accuracy improvement [40]. In time domain CS-based CE [15, 16, 41–44], the received pilot signals are transformed first into time domain for observation signal, and then an iterative recovery algorithm e.g., OMP [45, 46], is performed to estimate the unknown CIR. The first part of this chapter will discuss the overview of compressed sensing. And then, the channel estimation for each receiver (next generation DTTB system and ISDB-T system) will be discuss in details.

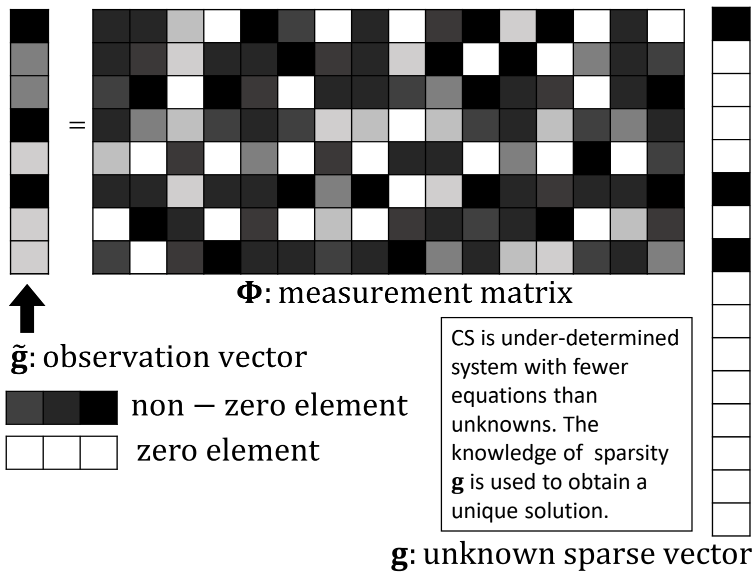

Figure 4.1: Linear model of compressed sensing

4.1 Overview of Compressed Sensing

CS is a recovery technique of a sparse signals using only few samples [16, 47]. CS method became popular in the field of imaging, magnetic resonance imaging (MRC), radar, data compression, and wireless communications where some signals involved are considered as sparse in nature [42]. In the case of wireless communication such as OFDM, CS can be applied for channel estimation with better accuracy and less pilot requirement. The main goal of CS is to locate the position of non-zeros in the unknown sparse vector.

The CS linear measurement model can be presented as

$$\tilde{\mathbf{g}} = \mathbf{\Phi}\mathbf{g}, \tag{4.1}$$

where $\tilde{\mathbf{g}}$ is the observation vector with size n, $\mathbf{\Phi}$ is the measurement matrix with size $n \times m$ given that $n < m$, and $\mathbf{g}$ is the unknown sparse vector with η non-zeros. Figure 4.1 shows the under-determined linear model of CS, where the number of unknowns is higher than the number of equations. The CS will be able to estimate the unknown $\mathbf{g}$ given the fact that $\mathbf{g}$ is always a sparse signal.

The recovery of the signal using CS will depends on sparsity of $\mathbf{g}$, the measurement matrix $\mathbf{\Phi}$, and the algorithm for CS. An important property of the measurement matrix of CS is the Restricted Isometry Property (RIP) introduced by Candes and Tao [48]. Based on this property, CS can successfully recover the sparse signal $\mathbf{g}$ if there exist a constant $(0 < \upsilon_k < 1)$ that satisfy the inequality

$$(1 - \upsilon_k)\|\mathbf{g}\|_2^2 \leq \|\mathbf{\Phi g}\| \leq (1 + \upsilon_k)\|\mathbf{g}\|_2^2, \tag{4.2}$$

where k is the order of RIP. Calculating the RIP of the measurement matrix is extremely difficult problem [15]. However, several measurement matrices have a higher probability of satisfying the RIP. An example is a measurement matrices whose columns are orthogonal such as discrete Fourier transform which is usually used for OFDM [49, 50].

The approach of obtaining the sparse solution of CS can be described in two ways namely: basis pursuit and greedy pursuit. The basis pursuit required L_p-norm to locate all the non-zeros of a sparse vector, but requires high computational cost. On the other hand, greedy approach uses iterative method to locate the position on non-zeros in the sparse vector and it has lower complexity with simple implementation.

4.1.1 Orthogonal Matching Pursuit

This research considers a greedy pursuit to determine the sparse solution of CS. An example of a greedy pursuit algorithms are matching pursuit (MP) and orthogonal matching pursuit (OMP). MP has lesser complexity but requires high number of iteration [51]. The OMP is capable of reducing the number of iteration of MP by implementing least-squares in every iteration to avoid choosing the same non-zero location [45]. Most of the greedy algorithm chooses OMP because of less execution time.

The objective of OMP is to solve the Eq.(4.1). Algorithm 1 shows the details of OMP algorithm. Finding the location of non-zero element of sparse vector can be done in $\lambda_i = \arg\max_k |\mathbf{r}_{i-1}^H \phi_k|$ where ϕ_k is the k-th column of measurement matrix $\mathbf{\Phi}$. At this point, an inner product between $\tilde{\mathbf{g}}$ and the columns of the measurement matrix $\mathbf{\Phi}$ was performed. And then, a least square $\arg\min_w ||\mathbf{Y}_i\mathbf{w} - \tilde{\mathbf{g}}||_2^2$ will be performed to estimate the amplitude value of the non-zero element of sparse vector. Next will performed the residual subtraction $\mathbf{r}_i = \tilde{\mathbf{g}} - \mathbf{Y}_i\mathbf{w}_i$ to ensure

Algorithm 1 Orthogonal Matching Pursuit (OMP)

Require: $\tilde{\mathbf{g}}$ ▷ observed vector

Ensure: $\mathbf{g}$ ▷ estimated sparse vector

$\mathbf{r}_i \leftarrow \tilde{\mathbf{g}}$

$\mathbf{\Phi} = \begin{bmatrix} \phi_0 & \phi_1 & \cdots & \phi_{N_{gi-1}} \end{bmatrix}$

$\mathbf{\Lambda}_i \leftarrow [\,]$

$\mathbf{Y}_i \leftarrow [\,]$

$i \leftarrow 1$

while $i \leq \eta$ **do**

  $\lambda_i = \arg\max_k |\mathbf{r}_{i-1}^H \phi_k|$

  $\mathbf{\Lambda}_i = \mathbf{\Lambda}_{i-1} \cup \{\lambda_i\}$

  $\mathbf{Y}_i = [\mathbf{Y}_{i-1}, \phi_{\lambda_i}]$

  $\mathbf{w}_i = \arg\min_w ||\mathbf{Y}_i \mathbf{w} - \tilde{\mathbf{g}}||_2^2$

  $\mathbf{r}_i = \tilde{\mathbf{g}} - \mathbf{Y}_i \mathbf{w}_i$

  $i = i + 1$

end while

return $\mathbf{g} = \mathbf{w}_\eta$

that different location of non-zero element will be chosen on the next iteration. The number of OMP iteration will depend on the sparsity η.

For the OMP complexity analysis, the 1st part of the algorithm is the inner product between the residual $\mathbf{r}$ and the measurement matrix $\mathbf{\Phi}$ represented as $\lambda_i = \arg\max_k |\mathbf{r}_{i-1}^H \phi_k|$ which has a complexity of $O((N_{gi})^2)$. And also, OMP has a LS represented as $\mathbf{w}_i = \arg\min_w ||\mathbf{Y}_i\mathbf{w} - \tilde{\mathbf{g}}||_2^2$ that has a complexity of $O(\eta^2 N_{gi})$ where η is the iteration. Summing up together, the total complexity of OMP is

$$O(\eta N_{gi}(N_{gi} + \eta^2)). \tag{4.3}$$

For the case of using OMP for CS, at least one of the following condition should be satisfied to guarantee that OMP can correctly recover the estimated impulse response [39]:

1. The $\mathbf{\Phi}$ in Eq.(4.2) should satisfy the RIP, with constant $\upsilon_{\eta+1} < \dfrac{1}{3\sqrt{\eta}}$ for order $\eta + 1$,
2. The mutual coherence μ of the measurement matrix $\mathbf{\Phi}$ should satisfy
$$\mu(\mathbf{\Phi}) \leq \frac{1}{2\eta - 1}, \tag{4.4}$$
where η is the maximum number of nonzero elements (sparsity level) of the unknown CIR vector $\mathbf{g}$.

In this research, we only consider the second condition in Eq.(4.4) about the mutual conherence of the measurmeent matrix. The mutual coherence indicates the correlation between the columns of the measurement matrix. The mutual coherence of the measurement matrix $\mathbf{\Phi}$ with the size n by m is defined as,

$$\mu(\mathbf{\Phi}) = \max_{1\leq i,j\leq m, i\neq j} \frac{||\phi_i^T \phi_j||}{||\phi_i||_2 \cdot ||\phi_j||_2}, \tag{4.5}$$

where ϕ_i is the i-th column of the measurement matrix $\mathbf{\Phi}$.

4.2 Channel Estimator for Next Generation DTTB System

This section will discuss the channel estimation for next generation DTTB receiver using CS. This process is necessary to estimate the channel matrix $\hat{\mathbf{H}}$ in

Eq.(3.9) of section 3.3.2. Although other channel estimation methods are also applicable in this system, CS was chosen because the channel is considered as sparse. CS is a popular technique for estimating a sparse information using only few measurements [16]. A sparse can be defined as a vector where most entries are zero and only few are non-zero. The sparse information that we are going to estimate is the CIR [18]. The CS equation can be defined as

$$\tilde{\mathbf{g}} = \mathbf{\Phi}\mathbf{g} + \mathbf{n}, \tag{4.6}$$

where $\tilde{\mathbf{g}}$, $\mathbf{\Phi}$, and $\mathbf{g}$ is the observed CIR vector, measurement matrix, and estimated CIR vector, respectively. We can estimate the CIR in Eq.(4.6) using the algorithm of CS called Orthogonal Matching Pursuit (OMP) [45].

Before estimating the channel, the receive pilot signals transmitted in Eq.(3.4) in section 3.2 are necessary. In order to avoid pilot interference from different antenna, the demodulator needs four different received signals in different time instant shown in Eq.(2.15) in previous section 2.2.1 for each receiving antenna. The observed CIR $\tilde{\mathbf{g}}_{i,j}$ for each channel $\mathbf{h}_{i,j}$ can be obtain using pilot extraction defined as

$$\tilde{\mathbf{g}}_{00} = \frac{1}{4}\mathbf{F}^{-1}\mathbf{E}\Big(\mathbf{y}_0^{(t)} - \mathbf{y}_0^{(t+1)} + \mathbf{y}_0^{(t+4)} - \mathbf{y}_0^{(t+5)}\Big), \tag{4.7}$$

$$\tilde{\mathbf{g}}_{01} = \frac{1}{4}\mathbf{F}^{-1}\mathbf{E}\Big(\mathbf{y}_0^{(t)} + \mathbf{y}_0^{(t+1)} + \mathbf{y}_0^{(t+4)} + \mathbf{y}_0^{(t+5)}\Big), \tag{4.8}$$

$$\tilde{\mathbf{g}}_{02} = \frac{1}{4}\mathbf{F}^{-1}\mathbf{E}\Big(\mathbf{y}_0^{(t+2)} + \mathbf{y}_0^{(t+3)} + \mathbf{y}_0^{(t+6)} + \mathbf{y}_0^{(t+7)}\Big), \tag{4.9}$$

$$\tilde{\mathbf{g}}_{03} = \frac{1}{4}\mathbf{F}^{-1}\mathbf{E}\Big(-\mathbf{y}_0^{(t+2)} + \mathbf{y}_0^{(t+3)} - \mathbf{y}_0^{(t+6)} + \mathbf{y}_0^{(t+7)}\Big), \tag{4.10}$$

$$\tilde{\mathbf{g}}_{10} = \frac{1}{4}\mathbf{F}^{-1}\mathbf{E}\Big(\mathbf{y}_1^{(t)} - \mathbf{y}_1^{(t+1)} + \mathbf{y}_1^{(t+4)} - \mathbf{y}_1^{(t+5)}\Big), \tag{4.11}$$

$$\tilde{\mathbf{g}}_{11} = \frac{1}{4}\mathbf{F}^{-1}\mathbf{E}\Big(\mathbf{y}_1^{(t)} + \mathbf{y}_1^{(t+1)} + \mathbf{y}_1^{(t+4)} + \mathbf{y}_1^{(t+5)}\Big), \tag{4.12}$$

$$\tilde{\mathbf{g}}_{12} = \frac{1}{4}\mathbf{F}^{-1}\mathbf{E}\Big(\mathbf{y}_1^{(t+2)} + \mathbf{y}_1^{(t+3)} + \mathbf{y}_1^{(t+6)} + \mathbf{y}_1^{(t+7)}\Big), \tag{4.13}$$

$$\tilde{\mathbf{g}}_{13} = \frac{1}{4}\mathbf{F}^{-1}\mathbf{E}\Big(-\mathbf{y}_1^{(t+2)} + \mathbf{y}_1^{(t+3)} - \mathbf{y}_1^{(t+6)} + \mathbf{y}_1^{(t+7)}\Big), \tag{4.14}$$

where $\mathbf{F}$ and $\mathbf{E}$ are the N-size FFT matrix and pilot arrangement matrix, respectively. The vector $\mathbf{y}_i$ is the OFDM received signal for all subcarriers of the i-th antenna in vector form with size N. The FFT matrix can be described as

$$\mathbf{F} = \frac{1}{\sqrt{N}}\left[\exp\left(-j\frac{2\pi kn}{N}\right)\right]_{\substack{0\leq k<(N-1)\\ 0\leq n<(N-1)}}, \tag{4.15}$$

while pilot arrangement matrix $\mathbf{E}$ is a diagonal matrix where the diagonal part contains $\mathbf{e} = \begin{bmatrix} e_0 & e_1 & \cdots & e_{N-1}\end{bmatrix}^T$. Each entries of $\mathbf{e}$ is defined as,

$$e_{Cm+i} = \begin{cases} \dfrac{1}{\mathrm{SP}_m} & (i=0) \\ 0 & (0<i<C) \end{cases}, \tag{4.16}$$

where $m \in \{0, ..., (M-1)\}$ and $C = \mathrm{round}(N/M)$. The SP_m is the m-th pilot symbol out of M total of pilots placed in OFDM subcarriers.

For the case of measurement matrix $\mathbf{\Phi}$, the measurement matrix is given by,

$$\mathbf{\Phi} = \mathbf{F}^{-1}\mathbf{Q}\mathbf{F}, \tag{4.17}$$

where $\mathbf{Q} = \mathrm{diag}(\mathbf{q}), \mathbf{q} = \begin{bmatrix} q_0 & q_1 & \cdots & q_{N-1}\end{bmatrix}^T$ that indicates the position of the pilots in the subcarriers. Each entries of $\mathbf{q}$ is defined as,

$$q_{Cm+i} = \begin{cases} 1 & (i=0) \\ 0 & (0<i<C) \end{cases}. \tag{4.18}$$

Finally, we can now estimate the CIR $\mathbf{g}$ of Eq.(4.6) using OMP algorithm. The OMP is a greedy method that aims stagewise minimization of the approximation error to the observed CIR [45].

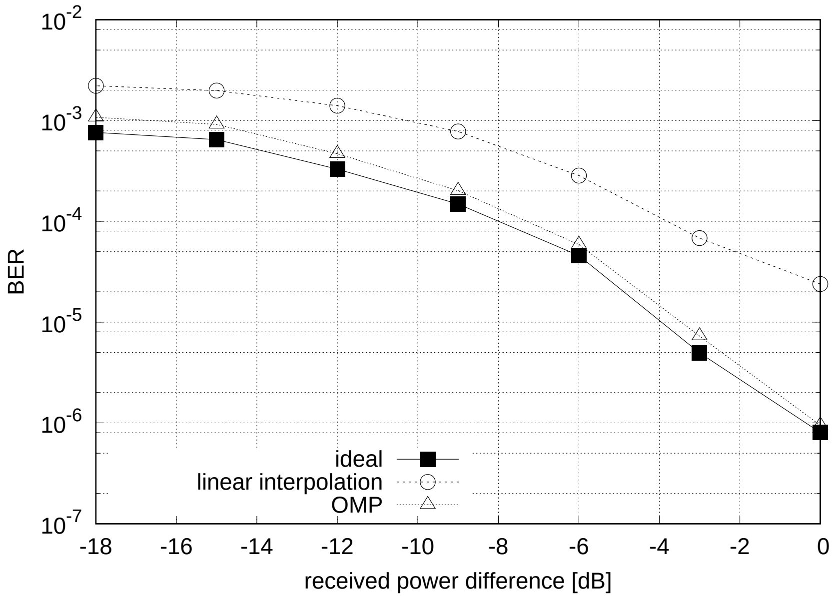

Figure 4.2: BER performance in 2 Rayleigh channel (base station Eb/No=25dB)

The algorithm 1 shows the details about the OMP. For the initialization of OMP, the algorithm needs only the observed CIR $\tilde{\mathbf{g}}$ and the number of iteration η. After obtaining the estimated CIR $\mathbf{g}$, the estimated channel can now be acquire by $\mathbf{F}^{-1}\mathbf{g}$. For the next generation DTTB system, the total number of channels to be estimated is 8 since there are 8 pairs of antennas from the transmitters to receiver.

In [3], the BER performance of the OMP was compared to perfect channel estimation (ideal) and linear interpolation. The performance was compared using multiple transmitters illustrated in Fig.2.7 of previous section 2.2.1 where the receiver receives different signal power for each transmitter. The received power difference is defined in Eq.(2.18) in previous section 2.2.1. Figure 4.2 shows BER performance of OMP compared to linear interpolation when the Eb/No=25dB. Here we can see that the error-rate of OMP outperformed the conventional linear interpolation. In addition, the performance of OMP is very close to ideal or perfect channel estimation.

Another simulation result in [3] is shown in Fig.4.3 where Eb/No=15dB. Similarly, the OMP outperforms the conventional linear interpolation even though the

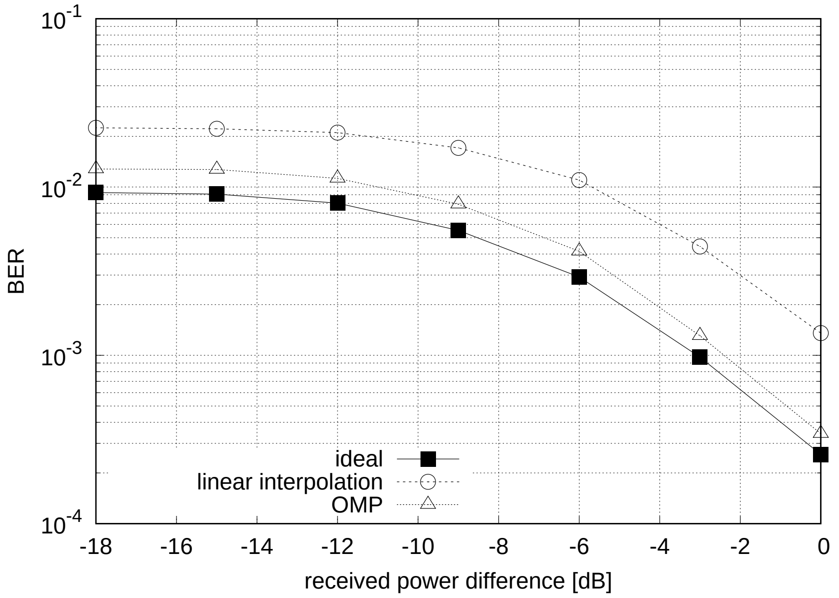

Figure 4.3: BER performance in 2 Rayleigh channel (base station Eb/No=15dB)

received signal power from different transmitters are low. And also, the error-rate of OMP is very close to ideal or perfect channel estimation. This suggest that channel estimation using CS is an ideal method compared to linear interpolation because the channel for DTTB system is sparse.

In [52], a simulations in terms of different signal to noise ratio was performed to compare the performance of OMP. Fig.4.4 shows the BER performance in 2 path Rayleigh channel. The OMP performance in time domain estimation is very close to the perfect channel estimation. And also, the OMP outperforms the linear interpolation by around 5 dB in Eb/No= 20dB.

Fig.4.5 shows the BER performance of OMP, linear interpolation and perfect channel estimation in Typical Urban 6 (TU6) channel. The OMP in time domain estimation BER performance is still close to the perfect channel estimation by only around 2dB performance gap in SNR=25dB. On the other hand, the linear interpolation cannot properly estimate the sparse channel that result to a higher BER especially in higher SNR as shown in the figure.

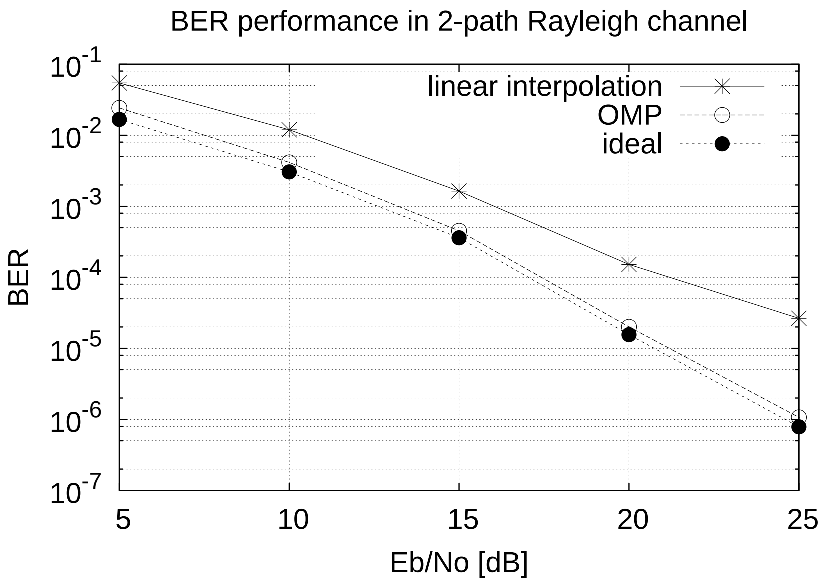

Figure 4.4: BER performance in 2 Rayleigh channel for different Eb/No values

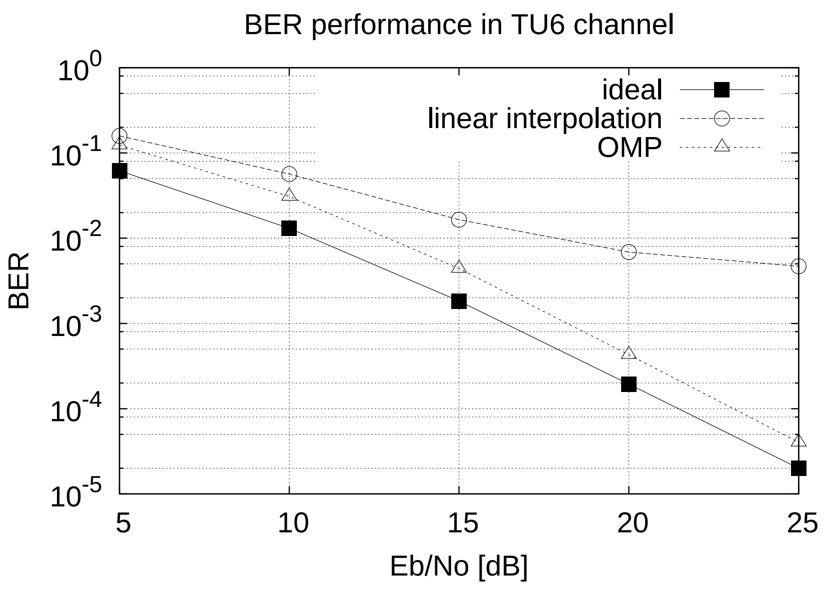

Figure 4.5: BER performance in TU6 channel for different Eb/No values

4.3 Channel Estimator for ISDB-T

The block diagram of the CS-based CE for ISDB-T is shown in Fig.4.6. Unlike the channel estimation for next generation DTTB system, channel estimation for ISDB-T is less complex and only one channel is required for estimation. That is because the number of receive antenna for ISDB-T is only one. After obtaining the received signal $\mathbf{v}$ from Eq.(2.9) previous section 2.1.1, the observed channel frequency response $\tilde{\mathbf{h}}$ can be obtained by

$$\tilde{\mathbf{h}} = \mathbf{E}\mathbf{v}, \tag{4.19}$$

where $\mathbf{E} = \mathrm{diag}(\mathbf{e})$ is a diagonal matrix. The vector $\mathbf{e}$ is defined as

$$\mathbf{e} = \begin{bmatrix} e_0 & e_1 & \cdots & e_{K-1} \end{bmatrix}^T, \tag{4.20}$$

wherein each entry of $\mathbf{e}$ is defined as

$$e_{Cm+i} = \begin{cases} \dfrac{1}{p_m} & (i=0) \\ 0 & (0 < i < C) \end{cases}, \tag{4.21}$$

where $m \in \{0, ..., M-1\}$. Here we extract the received pilots and compare with the known pilots.

After receiving the pilot signal, the N-size observed impulse response vector $\tilde{\mathbf{g}}$ can now be calculated as follows

$$\tilde{\mathbf{g}} = \mathbf{F}^{-1}\mathbf{Q}\tilde{\mathbf{h}} = [\tilde{g}_0, \tilde{g}_1, \cdots, \tilde{g}_{N-1}]^T. \tag{4.22}$$

In theory, the unknown frequency response $\mathbf{h}_s$ of the pilots can be modeled by using an unknown CIR $\mathbf{g} = [g_0, g_1, \cdots, g_{N-1}]^T$ using

$$\mathbf{h}_s = \mathbf{Q}_s\mathbf{Q}^T\mathbf{F}(\mathbf{g} + \mathbf{z}), \tag{4.23}$$

where $\mathbf{z}$ is the noise component and $\mathbf{Q}_s = \mathrm{diag}(\mathbf{q}_s), \mathbf{q}_s = \begin{bmatrix} q_0 & q_1 & \cdots & q_{K-1} \end{bmatrix}^T$ contains the pilot pattern. Each entry of $\mathbf{q}_s$ is defined as

$$q_{Cm+i} = \begin{cases} 1 & (i=0) \\ 0 & (0 < i < C) \end{cases}. \tag{4.24}$$

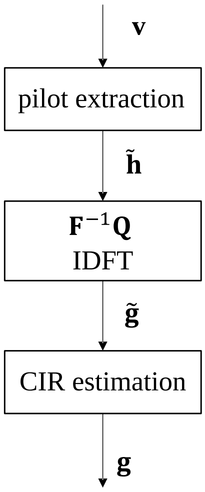

Figure 4.6: Block diagram of CS-based CE for ISDB-T

where $m \in \{0, ..., M-1\}$. The Eq.(4.22) and Eq.(4.23) are independent equations because the Eq.(4.22) is the observation part of CS equation. While Eq.(4.23) is the unknown part of CS equation.

At this point, we can combine the unknown frequency response $\mathbf{h_s}$ in Eq.(4.23) to the observed frequency response $\tilde{\mathbf{h}}$ in Eq.(4.22) to obtain the CS equation defined as

$$\tilde{\mathbf{g}} = \mathbf{F}^{-1}\mathbf{Q}\mathbf{Q}_s\mathbf{Q}^T\mathbf{F}(\mathbf{g} + \mathbf{z}). \tag{4.25}$$

We can define the measurement matrix $\mathbf{\Phi}$ as

$$\mathbf{\Phi} = \mathbf{F}^{-1}\mathbf{Q}\mathbf{Q}_s\mathbf{Q}^T\mathbf{F} \tag{4.26}$$

which is a band matrix. Eq.(4.25) can now be simplified to

$$\tilde{\mathbf{g}} = \mathbf{\Phi}\mathbf{g} + \mathbf{z}_l, \tag{4.27}$$

where

$$\mathbf{z}_l = \mathbf{\Phi}\mathbf{z}, \tag{4.28}$$

is the converted noise component.

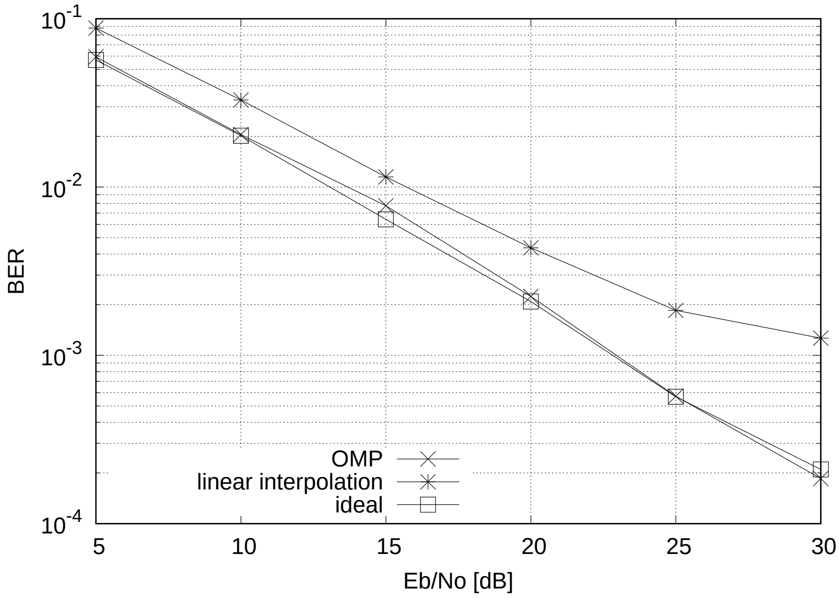

Figure 4.7: BER performance in 2 Rayleigh channel

The non-zero terms of $\tilde{\mathbf{g}}$ will be within the guard interval window because of the assumption that the maximum delay spread of the channel is within the guard interval. Therefore the observed impulse response $\tilde{\mathbf{g}}$ and the unknown impulse response $\mathbf{g}$ can be reduced to a vector of size equal to a guard interval N_{gi}. The observed impulse response will now be

$$\tilde{\mathbf{g}} = [\tilde{g}_0, \tilde{g}_1, \cdots, \tilde{g}_{N_{gi}-1}]^T, \tag{4.29}$$

and will then be used as an observation vector of CS. While the unknown CIR is

$$\mathbf{g} = [g_0, g_1, \cdots, g_{N_{gi}-1}]^T. \tag{4.30}$$

The Eq.(4.27) can now we solved using OMP in algorithm 1. The OMP is the same algorithm used for CS in next generation DTTB system in the previous section.

In [53], the BER performance of OMP in ISDB-T was compared with perfect channel estimation (ideal) and conventional linear interpolation as shown in Fig.4.7. Here we can observed that the OMP outperforms the linear interpolation. In addition, the OMP is very close to the performance of ideal or perfect channel estimation. The OMP outperforms the linear interpolation because the channel is sparse where compressed sensing using OMP is the preferred channel estimation method.

4.4 Summary

This chapter discusses the channel estimation method for next generation DTTB system and ISDB-T. The channel estimation difference for next generation DTTB system and ISDB-T is the required number channels to estimate. The ISDB-T will only estimate one channel in every receive signal because ISDB-T has only single receive antenna. On ther other hand, the next generation DTTB system requires 8 channels every receive signal because next generation DTTB system implements MIMO technique.

Both systems use the same type of channel which is a "sparse" channel where Compressed Sensing was implemented in estimating the channel. Compressed sensing is a reconstruction technique for a sparse information. The channel for DTTB system was considered a sparse channel where it composes of multi-path but few paths have higher signal power.

In order to lessen the complexity of compressed sensing, a time domain channel estimation was performed because estimating the channel in time domain will only reconstruct the channel impulse response. On the other hand, frequency domain channel estimation requires the high complexity because of the higher number of frequency subcarriers of OFDM that needs to estimate.

In addition, the Orthogonal Matching Pursuit was applied as an algorithm for compressed sensing. The OMP is a greedy pursuit algorithm for CS which is very simple to implement in terms of complexity requirement compared to other basis pursuit algorithm for CS. BER performance shows that OMP outperforms the conventional linear interpolation. And also, the OMP is very close to ideal or perfect channel estimation based on the simulation results.

5 Low-Complexity CS-based CE with Virtual Oversampling for ISDB-T

Using OMP as discussed in the previous chapter, a successful reconstruction of the unknown CIR can be guaranteed if mutual coherence [17] of the measurement matrix is less than or equal to $1/(2\eta - 1)$, where η is the number of nonzeros in the unknown CIR vector. However, under existence of fractional delay wherein the delay time of each path cannot be perfectly sampled by the symbol rate, the number of nonzero elements of the CIR observation vector increases which includes some fabricated paths, making the recovery algorithm less likely to converge. The fabricated paths happen because the path energy will leak to all other taps making the CIR no longer sparse [54].

Fractional delay exists in a system that uses time domain based channel estimation. Fractional delay in ISDB-T is a sampling time error of the channel delay. In an ISDB-T system, channel is a sparse wherein channel consists of multiple paths but few paths have higher power. Due to the existence of fractional delay, the CIR vector in time domain will include large number of fabricated paths which make the CS-based algorithms difficult to detect the real paths of CIR since the observation vector is no longer sparse. In order to remove the impact of the fractional delay, recently, the researcher proposed the time-domain oversampling in the previous papers [19] and [55]. However, an increase of transmission bandwidth happens in oversampling [56–58] since oversampling is performed in the transmitter side.

The goal of this chapter is to remove the impact of fractional delay in ISDB-T system. In addition, the signal bandwidth should not increase unlike the oversampling method. The contributions can be summarized as

1. A virtual oversampling using oversized Discrete Fourier Transform (DFT) matrix in the OMP processing is proposed to alleviate the impact of fractional delay. Using virtual oversampling, the number of nonzero elements of the unknown CIR vector decreases resulting in an increase of probability of successful reconstruction. The proposed virtual oversampling does not increase system bandwidth because it is carried only in the OMP processing at the receiver. A theoretical basis is provided on how the proposed virtual oversampling can mitigate the impact of fractional delay.

2. A modified OMP was proposed to reduce the computational complexity of OMP. The Modified Orthogonal Matching Pursuit (MOMP) can reduce the computational cost using the assumption that the rate of change of path delay is slower than the path gain in ISDB-T wireless channel. [59].

5.1 Fractional delay issue

This section will discuss the fractional delay issue. The issue will be explain in different views such as frequency domain, time domain, and non-sampled-spaced multipath delay.

5.1.1 Issue in frequency domain

The channel frequency response was described in Eq.(2.10) of previous section 2.1.1 about ISDB-T system model. This equation was derived as

$$\begin{aligned} h(f) &= \int_{-\infty}^{\infty} h(t)\exp(-j2\pi ft)dt \\ &= \int_{-\infty}^{\infty} \sum_{l=0}^{L-1} h_l\delta(t-\tau_l)\exp(-j2\pi ft)dt \\ &= \sum_{l=0}^{L-1} \int_{-\infty}^{\infty} h_l\delta(t-\tau_l)\exp(-j2\pi ft)dt. \\ &= \sum_{l=0}^{L-1} h_l\exp(-j2\pi\tau_l f) \\ h\Big(\frac{n}{NT_s}\Big) &= \sum_{l=0}^{L-1} h_l\mathrm{exp}\Big(-j\frac{2\pi n\tau_l}{NT_s}\Big) \end{aligned} \tag{5.1}$$

where $0 \leq n < (N-1)$. Since n is an integer number, the condition of $n = \tau_l/T_s$ is not always fulfilled because the delay τ_l is sometimes not a multiple of T_s as described to be $\tau_l = nT_s$. Therefore, we define a fractional delay wherein the τ_l/Ts is not an integer number.

5.1.2 Issue in time domain

Considering the observed CIR $\tilde{\mathbf{g}}$ from Eq.(4.29) in section 4.3 about ISDB-T channel estimation, the entries of $\tilde{\mathbf{g}}$ can be represented as

$$\tilde{g}_k = \frac{1}{N}\sum_{n=0}^{N-1}\sum_{l=0}^{L-1} h_l\mathrm{exp}\Big(-j\frac{2\pi n\tau_l}{NT_s} + j\frac{2\pi nk}{N}\Big), \tag{5.2}$$

where $0 \leq k < (N_{gi}-1)$. Now let us define a delay τ_l of the l-th path to be

$$\tau_l = \zeta_l T_s + \Delta\tau_l \tag{5.3}$$

where ζ_l, $\Delta\tau_l$ is an integer number and fractional delay of the l-th path $l \in \{0, ..., L-1\}$, respectively. The fractional delay is assumed to be within the range of $0 \leq \Delta\tau_l < T_s$. Substituting Eq.(5.3) into Eq.(5.2) we get

$$\tilde{g}_k = \frac{1}{N}\sum_{n=0}^{N-1}\sum_{l=0}^{L-1} h_l\mathrm{exp}\Big(-j\frac{2\pi n\Delta\tau_l}{NT_s}\Big)\mathrm{exp}\Big(-j\frac{2\pi n}{N}(\zeta_l - k)\Big). \tag{5.4}$$

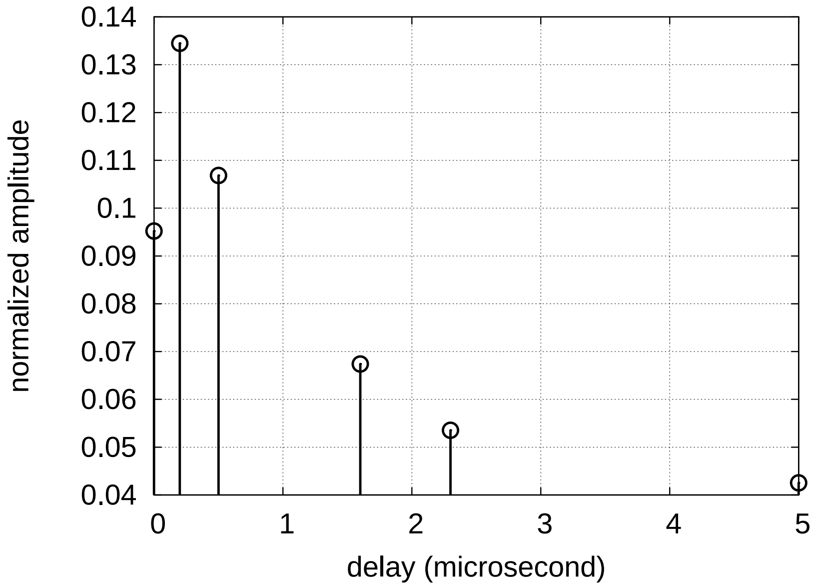

Figure 5.1: Observed channel impulse response $\tilde{\mathbf{g}}$ of TU6 channel without fractional delay using $T_s = 0.10\mu s$

If the fractional delay $\Delta\tau_l = 0$, the Eq.(5.4) will be

$$\begin{aligned}\tilde{g}_k &= \frac{1}{N}\sum_{n=0}^{N-1}\sum_{l=0}^{L-1} h_l \exp\Big(-j\frac{2\pi n}{N}(\zeta_l - k)\Big) \\ &= \begin{cases} h_l & ;(\zeta_l = k) \\ 0 & ;(\zeta_l \neq k), \end{cases}\end{aligned} \quad . \tag{5.5}$$

Figure 5.1 shows observed CIR $\tilde{\mathbf{g}}$ in TU6 channel model without fractional using $T_s = 0.10\mu s$. Here we can see that the observed CIR $\tilde{\mathbf{g}}$ is sparse in the case without fractional delay. The $T_s = 0.10\mu s$ does not have fractional delay effect to the observed CIR because it is perfectly divisible with the delays of the TU6 channel. Without fractional delay, the observed CIR is sparse and can easily measure the delay using compressed sensing.

For the case of existing fractional delay where $\Delta\tau_l \neq 0$. The CIR with $\zeta_l = k$ will be,

$$\tilde{g}_k = \frac{1}{N}\sum_{n=0}^{N-1}\sum_{l=0}^{L-1} h_l \exp\Big(-j\frac{2\pi n \Delta\tau_l}{NT_s}\Big), \tag{5.6}$$

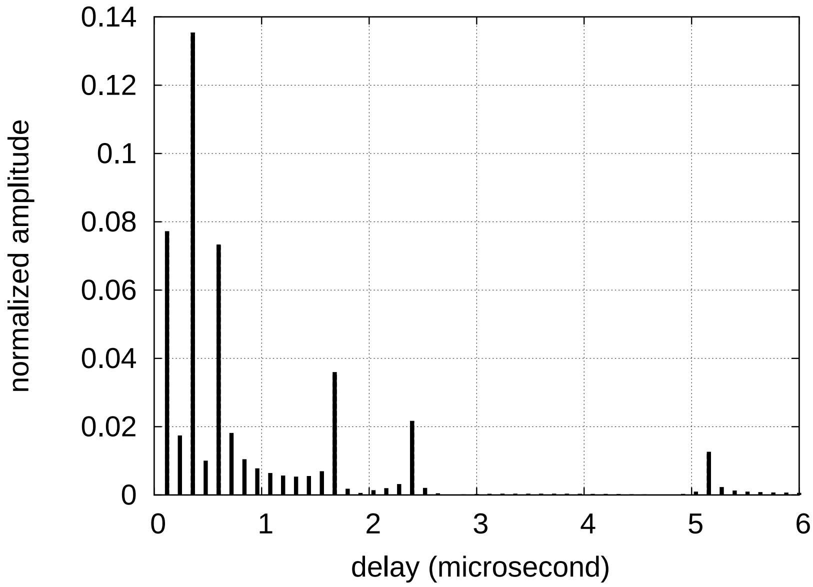

Figure 5.2: Observed channel impulse response $\tilde{\mathbf{g}}$ of TU6 channel in the presence of fractional delay using $T_s = 0.12\mu s$

and if $\zeta_l \neq k$, the CIR will be

$$\tilde{g}_k = \frac{1}{N} \sum_{n=0}^{N-1} \sum_{l=0}^{L-1} h_l \exp\Big[\Big(- j\frac{2\pi n}{N}\Big)\Big(\zeta_l - k + \frac{\Delta\tau_l}{T_s}\Big)\Big]. \tag{5.7}$$

Here we can see that Eq.(5.7) is no longer zero because of the presence of $\frac{\Delta\tau_l}{T_s}$ which is a fractional number. The fractional delay will create additional impulses that would result for the observed CIR to be non-sparse. This happens because the path energy will leak to all other taps making the CIR to be non-sparse.

An effect of the fractional delay to the observed CIR $\tilde{\mathbf{g}}$ in TU6 channel model using $T_s = 0.12\mu s$ is shown in Fig.5.2. The ideal TU6 channel model has 6 paths as demonstrated in table 3.3. Table 3.3 shows the corresponding power and delay of each path of the ideal TU6 channel. Figure 5.2 shows the normalized amplitude of each impulses of CIR defined as $|\tilde{\mathbf{g}}|$, versus the measured delay time. The 6 paths of TU6 channel appear as a high normalized amplitude impulses in Fig.5.2. Ideally, the CIR should only be 6 impulses. Due to the effect of fractional delay, a small impulses were generated as shown in Fig.5.2. The small impulses are

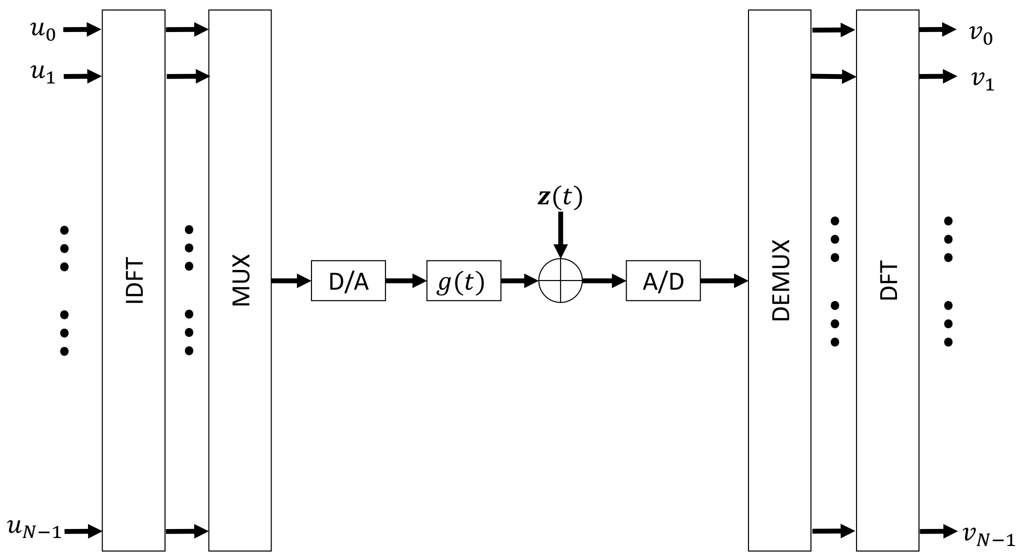

Figure 5.3: Based-band OFDM system [5]

defined in Eq.(5.7). The additional small impulses will result for the observed CIR to be non-sparse and the number of path is no longer equal to L. In addition, the 6 paths of TU6 cannot perfectly measure the correct delay due to non-sparsity of the CIR.

5.1.3 Non-sampled-spaced multipath delay

In [5], the effect of fractional delay was described in terms of non-sampled-spaced multipath delay. The channel impulse response is described to be a time-limited pulse train defined as

$$g(t) = \sum_{m=0}^{M} h_m \delta(t - \tau_m T_s) \tag{5.8}$$

where h_m is the complex amplitude and $\tau_m T_s$ is the delay. The system model is described in Fig.5.3 where the received signal $\mathbf{v} = [v_0, v_1, \cdots, v_{N-1}]^T$ is described as

$$\mathbf{v} = \mathrm{DFT}_N\Big(\mathrm{IDFT}_N\big(\mathbf{u}\big) * \frac{\mathbf{g}}{\sqrt{N}} + \mathbf{z}\Big). \tag{5.9}$$

The transmitted signal $\mathbf{u} = [u_0, u_1, \cdots, u_{N-1}]^T$ is transformed using N-point inverse discrete-time Fourier transform (IDFT_N) before convolution ($*$) with $\mathbf{g}$.

Because of the fact that the CIR in Eq.(5.8) is time-limited, transforming it in frequency domain will span the whole frequency domain. However, OFDM receiver is frequency limited for certain bandwidth and it will sample the OFDM signal in frequency domain [60]. In this case, the $\mathbf{g} = [g_0, g_1, \cdots, g_{N-1}]^T$ in Eq.(5.9) will be

$$g_k = \frac{1}{\sqrt{N}} \sum_{m=0}^{M} h_m \exp\Big(- j\frac{\pi}{N}\Big(k + (N-1)\tau_m\Big)\Big) \frac{\sin\Big(\pi\tau_m\Big)}{\sin\Big(\frac{\pi}{N}(\tau_m - k)\Big)}. \tag{5.10}$$

In [5], the τ_m is restricted to be an integer number to avoid the fractional delay issue as shown in Fig.5.2 which is not always true in practical situation. But in this chapter, we consider a non-integer of τ_m as defined to be fractional delay. Here we can see that the CIR is no longer time limited because of sinc function. In addition, since the sampling is perform in frequency domain, the impulse response will be shifted and added up resulting to a fractional delay effect as shown in Fig.5.2 if τ_m is not an integer number. This phenomenon is known as path energy leakage of all other channel taps in non-sampled-spaced multipath delay.

5.2 CS-based CE with Virtual Oversampling

To mitigate impact of fractional delay, a proposed virtual oversampled unknown CIR vector $\mathbf{g}_X = [g_{X,0}, g_{X,1}, \cdots, g_{X,XN-1}]^T$ was introduced in this section. One should note that the word "virtual" stems from the fact that the proposed oversampling is virtually implemented only within the measurement matrix in CS and does not increase system bandwidth of ISDB-T during transmission.

The parameter X is introduced to represent how many times the unknown vector is virtually oversampled. Let us define the X times oversized DFT and reorder matrices as,

$$\mathbf{F}_X = \frac{1}{\sqrt{XN}} \left[\exp\left(-j\frac{2\pi kn}{XN}\right)\right]_{\substack{0 \le k < (XN-1) \\ 0 \le n < (XN-1)}}, \tag{5.11}$$

and

$$\mathbf{Q}_X = \begin{bmatrix} \mathbf{0}_{(K/2)\times(K/2)} & \mathbf{I}_{K/2} \\ \mathbf{0}_{(XN-K)\times(K/2)} & \mathbf{0}_{(XN-K)\times(K/2)} \\ \mathbf{I}_{K/2} & \mathbf{0}_{(K/2)\times(K/2)} \end{bmatrix}. \tag{5.12}$$

The unknown frequency response $\mathbf{h}_X$ of Eq.(4.23) with virtual oversample can be now calculated using the unknown CIR $\mathbf{g}_X = [g_{X,0}, g_{X,1}, \cdots, g_{X,XN-1}]^T$ with vector size of XN using

$$\mathbf{h}_X = \mathbf{Q}_s\mathbf{Q}_X^T\mathbf{F}_X(\mathbf{g}_X + \mathbf{z}_X), \tag{5.13}$$

The unknown frequency response $\mathbf{h}_X$ with virtual oversampling is then subtitute to the observed frequency response $\tilde{\mathbf{h}}$ in Eq.(4.22) to obtain the CS equation defined as

$$\tilde{\mathbf{g}} = \mathbf{F}^{-1}\mathbf{Q}\mathbf{Q}_s\mathbf{Q}_X^T\mathbf{F}_X(\mathbf{g}_X + \mathbf{z}_X). \tag{5.14}$$

Finally we can define the measurement matrix $\mathbf{\Phi}_X$ with virtual oversampling as

$$\mathbf{\Phi}_X = \mathbf{F}^{-1}\mathbf{Q}\mathbf{Q}_s\mathbf{Q}_X^T\mathbf{F}_X, \tag{5.15}$$

which is a band matrix with a size of N by XN. Equation (5.14) can now be simplified to

$$\tilde{\mathbf{g}} = \mathbf{\Phi}_X\mathbf{g}_X + \mathbf{z}_{Xl}, \tag{5.16}$$

where

$$\mathbf{z}_{Xl} = \mathbf{\Phi}\mathbf{z}_X, \tag{5.17}$$

is the converted noise component.

With the proposed virtual oversampling, we can now detect accurately the actual channel delay and eliminate the effect of fractional delay. Each entries of the estimated CIR $\mathbf{g}_X$ will be defined as

$$g_{X,k}=\frac{1}{N}\sum_{n=0}^{XN-1}\sum_{l=0}^{L-1}h_l\exp\Big[\Big(-j\frac{2\pi n}{N}\Big)\Big(\frac{\zeta_l-k}{X}+\frac{\Delta\tau_l}{T_s}\Big)\Big] \tag{5.18}$$

where $(0 \leq k < XN_{gi}-1)$. Here we observed that we increased the size of the estimated CIR $\mathbf{g}_X$ to XN_{gi} using virtual oversampling which is part of the measurement matrix being used.

In the case of the presence of fractional delay where $\Delta\tau_l \neq 0$, the term $\Big(\frac{\zeta_l-k}{X}+\frac{\Delta\tau_l}{T_s}\Big)$ in Eq.(5.18) is now an integer number that will result for $g_{X,k}$ to be equal to zero in the case of $\zeta_l \neq k$. And the estimated CIR with virtual oversample $\mathbf{g}_X$ will be simplify to

$$g_{X,k}=\frac{1}{N}\sum_{n=0}^{XN-1}\sum_{l=0}^{L-1}h_l\exp\Big(-j\frac{2\pi n\Delta\tau_l}{NT_s}\Big) \tag{5.19}$$

for $\zeta_l = k$, and

$$g_{X,k}=0 \tag{5.20}$$

for $\zeta_l \neq k$. With the presence of fractional delay, here we can observe that the estimated CIR $\mathbf{g}_X$ is already a sparse again where the number of nonzeros of $\mathbf{g}_X$ was reduced to L.

To verify whether a given measurement matrix with virtual oversampling guarantees the recovery of CIR, at least one of the condition in section 4.1.1 should satisfy. This research will only consider the second condition stated in Eq.(4.4). The virtual oversampling is performed to reduce the number of nonzero elements η of the unknown CIR vector to L so that the OMP is more likely to converge according to the condition for successful reconstruction given in Eq.(4.4).

For the worst case scenario, let us consider the mutual coherence to be $\mu(\mathbf{\Phi}_X) = \frac{1}{2\eta-1}$. Let us also consider a parameters based on ISDB-T One-Seg given in table 5.1 and a virtual oversampling factor $X = 4$. Computing the mutual coherence using Eq.(4.5) will result to $\mu(\mathbf{\Phi}_4) = 0.0174$, which leads to a value $\eta \approx 29$. A $\eta \approx 29$ means the proposed measurement matrix can estimate up to 29 number of channel paths. A limitation of 29 paths is enough since the channel model of ISDB-T is only composed of 6 paths such as TU6 and hilly terrain model.

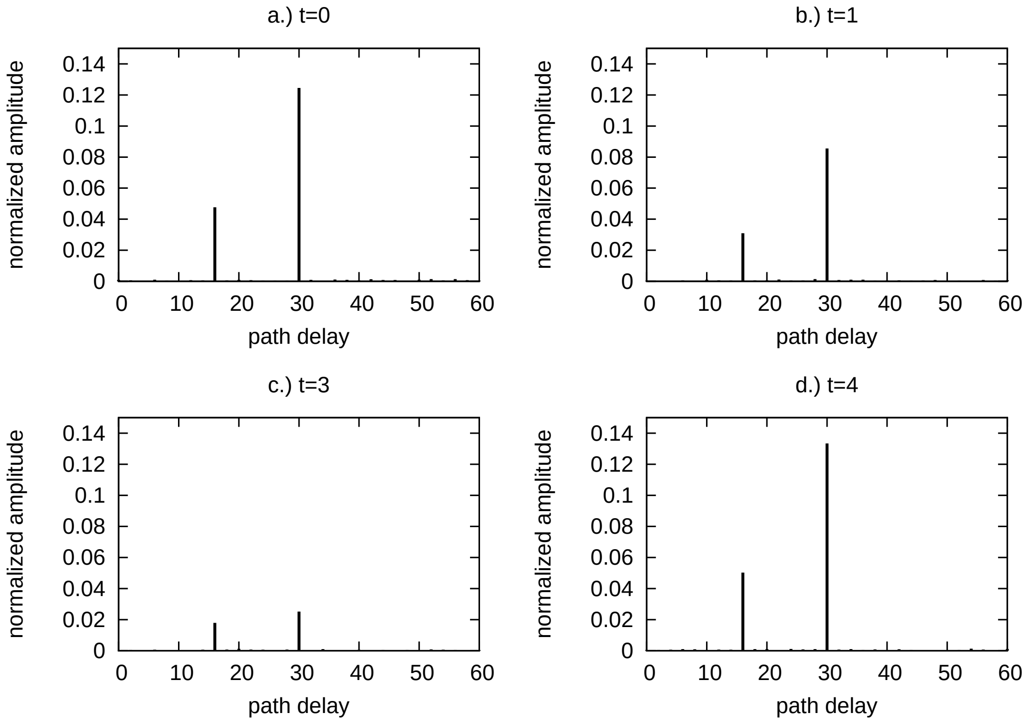

Figure 5.4: Channel impulse response for different time instances

5.2.1 Modified Orthogonal Matching Pursuit

In [59], it discussed that the rate of change of the delay of l-path is slower compared to the amplitude response h_l where $l \in \{0, ..., L-1\}$. Figure 5.4 shows the CIR for time $t = 1, 2, 3, 4$ in two Rayleigh channel. Here we can observe that the impulse position does not change because the delay paths of the channel is constant for some time instances. Only the impulse gain or the path gain is changing over time instances. We can exploit this assumption in order to reduce the complexity in CIR estimation.

Doing this, a Modified Orthogonal Matching Pursuit (MOMP) will be the proposed algorithm for CS. The algorithm is composed of two parts namely the Orthogonal Matching Pursuit (OMP) [45], and the Least Square (LS). The CIR estimation has two parts wherein the first part will use the OMP to estimate the both gain and delay path of the first symbol arrival. And then for the second

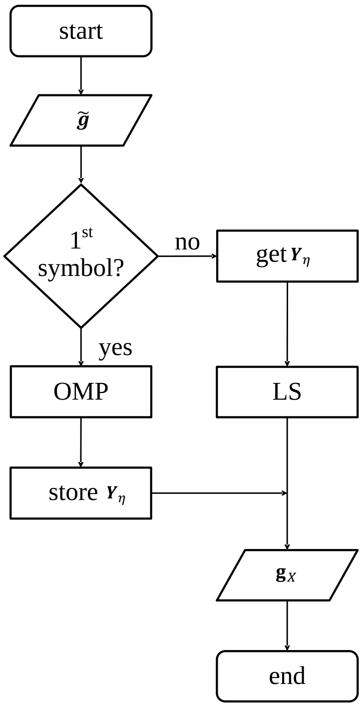

Figure 5.5: System flow chart of MOMP

part, since the delay path is slowly changing compared to the amplitude response, the rest of the symbol will only estimate the gain using LS with the supports of the computed OMP at first part.

The flow chart of the MOMP is shown in Fig.5.5. The OMP will be used first for the 1st symbol arrival to estimate the delay and gain of the multipath channel. The delay information is available in the search boundary selector $\mathbf{Y}_\eta$ which will then be used for the next symbol arrival. For the succeeding symbol arrival, the LS will be used to estimate only the gain of the channel using the $\mathbf{Y}_\eta$ of OMP. With MOMP, it is expected that the complexity will be reduced in estimating the CIR.

OMP based Gain and Delay Estimator

The Algorithm 1 in section 4.1.1 shows the detailed steps of the OMP algorithm [45] for obtaining the search boundary selector $\mathbf{Y}_\eta$ and solving the impulse response $\mathbf{g}_X$ of the Eq.(5.16). Orthogonal Matching Pursuit (OMP) is a greedy algorithm that aims stagewise minimization of the approximation error to the observed signal [45]. The OMP is an iterative algorithm where the number of iteration used is equal to η, the number of nonzero elements of $\mathbf{g}_X$. OMP will be used only for the first symbol arrival to estimate both the delay and gain paths of the channel.

Due to virtual oversampling, the columns of the measurement matrix represented by ϕ_k were increased and will result to a high resolution testing. The OMP can effectively detect the channel delay by finding the maximum inner product λ_i. In the OMP algorithm, the $\lambda_i = \arg\max_k |\mathbf{r}_{i-1}^H \phi_k|$ detects accurately the channel delay and eliminates the smaller impulses generated by fractional delay as discussed in section 5.1.

LS Based Gain Estimator

According to [59], the delay of the channel is changing slower compared to the gain. This assumption is also shown in Fig.5.4. In this case, estimating the delay is not necessary because the delay estimation has completed at the first part using OMP. Therefore, only gain is required to estimate for the next symbol arrival. The LS will be used as a gain estimator of each path after OMP.

The LS [59] will be used to estimate the path gains of the channel. The estimated impulse response $\mathbf{g}_X \in \mathbb{C}^{XN_{gi}}$ will be estimated using

$$\mathbf{g}_X = (\mathbf{Y}_\eta^H \mathbf{Y}_\eta)^{-1} \mathbf{Y}_\eta^H \tilde{\mathbf{g}}. \tag{5.21}$$

Using the support of the measurement matrix $\mathbf{Y}_\eta$ in OMP in Algorithm 1, we can reduce the complexity of LS because the column size of the matrix $\mathbf{Y}_\eta$ is only equal to η. The support of the OMP $\mathbf{Y}_\eta$ will be the search boundary selector since it searches the columns of the measurement matrix that will be used in LS estimator. With this improvement, the iteration will be reduced into a single iteration instead of using multiple iteration.

Complexity Analysis

So far, the computational cost of MOMP was reduced as follows.

1. Since we reduced the size of the observed impulse response $\tilde{\mathbf{g}}$ to a size equal to a guard interval N_{gi} as mentioned in section 4.3, we also need to reduce the size of the unknown CIR $\mathbf{g}_X$ and measurement matrix $\mathbf{\Phi}_X$ for consistency. This size reduction is based on the assumption that the maximum delay spread of the channel is within the size of the guard interval N_{gi}. The reduced virtually oversampled impulse response vector now becomes

$$\mathbf{g}_X = \begin{bmatrix} g_{X,0} & g_{X,1} & \cdots & g_{X,XN_{gi}-1} \end{bmatrix}^T, \tag{5.22}$$

and the corresponding measurement matrix becomes

$$\mathbf{\Phi}_X = \left[\Phi_{i,n}\right]_{\substack{0 \leq i < (N_{gi}-1) \\ 0 \leq n < (XN_{gi}-1)}}, \tag{5.23}$$

The new size of the measurement matrix $\mathbf{\Phi}_X$ is now N_{gi} by XN_{gi} where N_{gi} is the size of the guard interval and X is the oversample factor that determines how many times the signal was oversampled. Note that the n-th column vector of $\mathbf{\Phi}_X$ corresponds to the finger-print of the band limited impulse response of the fractional delayed path. This size reduction of the measurement matrix and the observation vector of CS is advantageous because it will result to a reduction in computational complexity.

2. According to section 5.2 that discusses about CS, the measurement matrix of the proposed system was a band matrix wherein almost all of the entries of the matrix are zeros. This will reduce the computational cost in OMP in algorithm 1 since OMP uses inner products of the columns of the measurement matrix. Using band measurement matrix will reduce the number of products since most of the entries of the column vector of the measurement matrix are zeros.

3. The algorithm that was used for compressed sensing is the MOMP which was discussed in section 5.2.1. MOMP is a low computational cost algorithm that uses only single iteration using LS with the support of OMP in the 1st symbol calculation. MOMP was proposed as an algorithm for CS because of the assumption that the delay path changes slowly compared to the gain of each path.

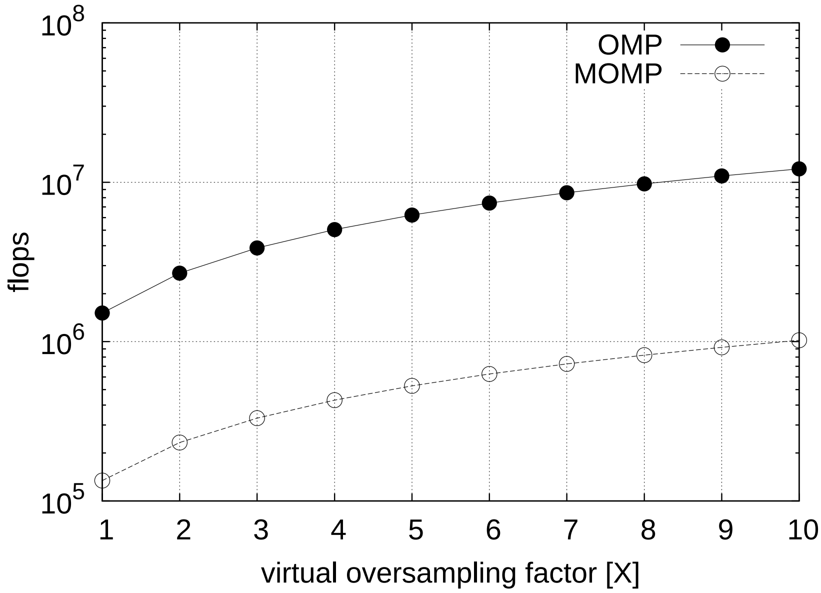

Figure 5.6: OMP vs. MOMP in terms of FLOP count

With the enumerated ways of reduction using the MOMP above, we can now analyze the complexity order of the proposed algorithm. The first part of MOMP is the estimation of delay and gain using OMP which has a complexity of $O(\eta N_{gi}(XN_{gi} + \eta^2))$ as discussed in Eq.(4.3) of section 4.1.1. Here we change the N_{gi} to XN_{gi} because of the increased size of measurement matrix due to virtual oversampling. For the 2nd part of the channel estimation using LS [59], the complexity is $O(\eta N_{gi})$. The total complexity of the MOMP is equivalent to

$$O(\eta N_{gi}(XN_{gi} + \eta^2 + 1)). \tag{5.24}$$

In order to fully understand the computational complexity, an example will be given where the $\eta = 6, N_{gi} = 128$ and $X = 2$ for 12 symbol arrival. Here we compare with the system wherein a conventional OMP will be used for all symbol arrival. For the case of OMP, the number of floating-point operations per second (FLOPS) using Eq.(4.3) will be $12 \times (6 \times 128 \times (2 \times 128 + 6^2)) = 2,691,072$.

For the case of MOMP, the FLOPS counts using Eq.(4.3) will be use only once such as $6 \times 128 \times (2 \times 128 + 6^2)) = 224,256$, while the remaining symbols will use the $O(\eta N_{gi})$ which is $11 \times 6 \times 128 = 8,448$. Then the overall FLOPS count for MOMP will be $224256 + 8448 = 232,704$. Comparing both method, the percentage complexity savings of MOMP in reference to full OMP will be 91.35%.

Figure 5.6 shows the FLOPS count of MOMP and OMP for different oversampling factor X. For the MOMP in this simulation, the channel estimation uses OMP for the 1st symbol while the other 11 symbols are using LS. The conventional OMP will be use for all 12 symbol arrival. Here we can see in the figure that the FLOPS count of MOMP is lesser compared to the conventional OMP because MOMP only uses OMP for first symbol arrival while most ot the symbol uses LS.

5.3 Simulation Results

The proposed method was evaluated in terms of normalized mean square error (NMSE) and BER performance. A C++ programming with IT++ library for communication systems was used to obtain the simulation results [35]. For simplicity reason, we consider ISDB-T One-Seg as a simulation parameters. Table 5.1 shows the simulation parameters wherein the ISDB-T One-Seg configuration was considered. The number of MOMP iteration η for both hilly terrain and TU6 is 6 since both channels have 6 paths. The sampling interval $T_s = 0.008\mu s$ was chosen to realize fractional delay for all channel models used in the simulation. The tables 3.3 and 5.2 show the delay profile of the channel model that were used in simulation. Based on the delay profile given, the value of T_s is not divisible with the delays of the channels which assure that fractional delay will occur.

5.3.1 NMSE performance

The normalized mean square error (NMSE) is a measure of estimated channel frequency response in comparison with the perfect channel frequency response. The NMSE is defined as,

$$NMSE = \frac{\sum_{k=0}^{K-1} |h'_k - h'_{X,k}|^2}{\sum_{k=0}^{K-1} |h'_k|^2}, \tag{5.25}$$

Table 5.1: Simulation parameters

System Model	ISDB-T One-Seg
channel model	TU6, hilly terrain
modulation type	QPSK
FFT size	$N = 512$
active subcarriers	$K = 432$
data subcarrier	$K - M = 396$
pilot subcarrier	$M = 36$
sampling interval	$T_s = 0.08\mu s$
pilot type	scattered type
noise type	AWGN
MOMP iteration	$\eta = 6 \rightarrow$ TU6, $\eta = 6 \rightarrow$ hilly terrain
OFDM symbols per frame	12
frames	10000
guard interval	$\frac{1}{4} \rightarrow$ TU6
	$\frac{1}{2} \rightarrow$ hilly terrain

Table 5.2: hilly terrain delay profile

delay (μs)	power (dB)
0	0
0.1	-1.5
0.3	-4.5
0.5	-7.5
15.0	-8
17.2	-17.7

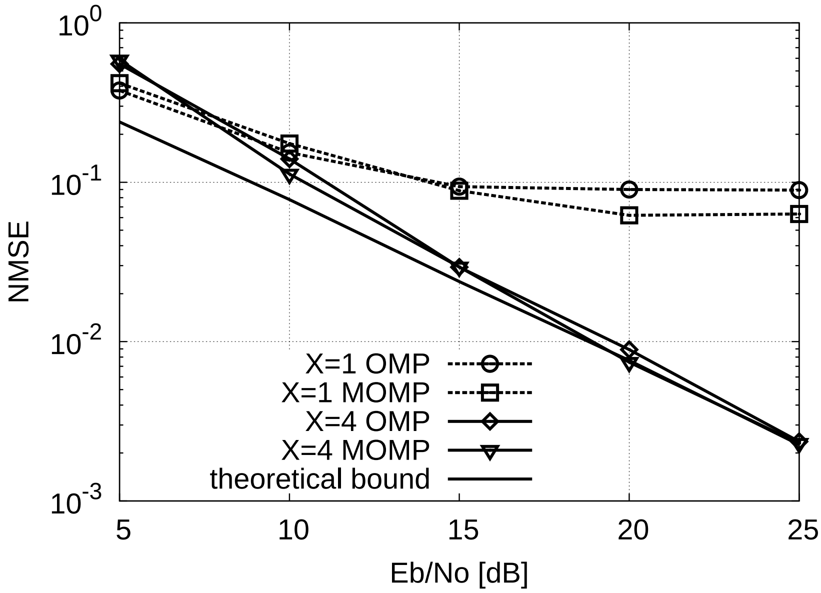

Figure 5.7: NMSE performance in TU6 channel

where $\mathbf{h}' = \mathbf{Q}^T\mathbf{h}$ is the actual channel frequency response and $\mathbf{h}'_X = \mathbf{Q}_X^T\mathbf{F}_X\mathbf{g}_X$ is the estimated channel frequency response. Figure 5.7 shows the NMSE of the estimated channel in typical urban channel. While Fig.5.8 shows the NMSE of the estimated channel in hilly terrain environment.

The NMSE performance of full OMP and MOMP for both Fig.5.7 and Fig.5.8 shows almost equal quality. The MOMP achieves the same accuracy with the full OMP for estimating the delay and gain of the channel even though MOMP has less complexity compared to OMP. The MOMP exploits the slow change of the delay path to reduce the channel estimation complexity.

For the urban channel shown in Fig.5.7, a high NMSE of about 0.2 from Eb/No=10 dB to Eb/No=25 dB in a system without virtual oversampling ($X = 1$). The fact that NMSE is not improved in non-oversample ($X = 1$) even when Eb/No is increased implies that the channel estimation error is dominated by the impact of fractional delay as mentioned in section 5.1. A virtual oversampling ($X = 4$) in the receiver side was performed to mitigate the impact of fractional delay which results to a better NMSE performance. Virtual oversampling ($X = 4$) indicates a successful construction of the CIR by mitigating the effect of frac-

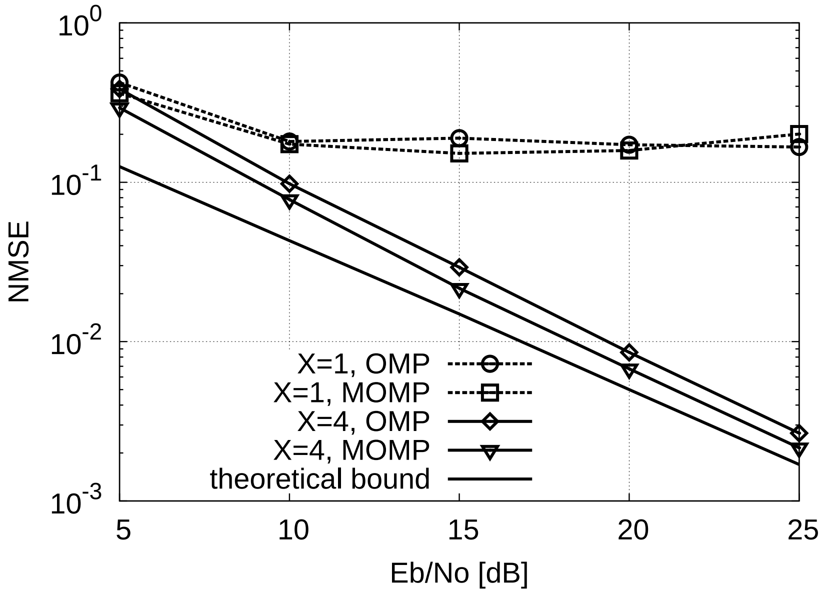

Figure 5.8: NMSE performance in hilly terrain

tional delay, which results in a significant improvement in NMSE as Eb/No is increasing.

For the hilly terrain shown in Fig.5.8, the NMSE performance shows almost the same results compared to urban terrain in Fig.5.7. The guard interval in hilly terrain was increased to $\frac{1}{2}$ because the delay spread of hilly terrain is wider compared to a TU6 channel. As expected, the Fig.5.8 shows that the NMSE without virtual oversampling ($X = 1$) has high error because of the presence of fractional delay. While the NMSE of virtual oversampling ($X = 4$) improves because it was able to detect the fractional delay.

In addition, a comparison between the proposed method and the theoretical lower bound of CS called oracle estimator [61, 62] was provided. The oracle estimator is composed of submatrix of the measurement matrix $\mathbf{\Phi}_X$. The columns of submatrix $\mathbf{Y}_{\eta'}$ of the oracle estimator are composed of correct test vectors that determine the correct time delay of the channel. The theoretical bound of the oracle estimator is defined as

$$\mathbf{h}_{oracle} = \mathbf{Q}_X^T \mathbf{F}_X (\mathbf{Y}_{\eta'}^H \mathbf{Y}_{\eta'})^{-1} \mathbf{Y}_{\eta'}^H \tilde{\mathbf{g}} \tag{5.26}$$

where $\mathbf{Y}_{\eta'}$ is the submatrix of the measurement matrix $\mathbf{\Phi}_X$, and η' are the indices that determine the correct test vectors of $\mathbf{\Phi}_X$. As shown in Fig.5.7 and Fig.5.8, the MOMP and theoretical bound converge each other in higher Eb/No region both for hilly terrain and TU6 channel.

For comparison between the proposed MOMP to the theoretical bound in TU6 channel as shown in Fig.5.7, the proposed MOMP is close to the theoretical bound especially in the higher Eb/No of 15dB to 25dB. The gap between the proposed MOMP and theoretical bound is only less than 2dB in lower Eb/No region in TU6 channel.

For the hilly terrain as shown in Fig.5.8, the proposed MOMP method is only less than 2dB difference compared to the theoretical bound in higher Eb/No region. The NMSE gap between the proposed MOMP and theoretical bound is higher in hilly terrain channel compared to TU6 channel because hilly terrain has higher delay spread of channel paths than TU6 channel. Higher delay spread of the channel would result to higher probability of not getting the correct delay time of the channel.

5.3.2 BER performance

The BER performance is detailed measurement method compared to NMSE performance because BER performance measures the error rate of the transmitted data while NMSE performance is only the error of channel estimation. The channel that was used during the simulation is the TU6 channel which has low delay spread, and the hilly terrain which has high delay spread. In addition, the modulation type that was used is QPSK with different virtual oversampling factor $X = 1, 2$ and 4.

For the TU6 channel shown in Fig.5.9, the non-virtual oversampling ($X = 1$) has higher error because of the presence of fractional delay. Increasing the value of virtual oversampling into $X = 2$ and $X = 4$ improves the BER performance. In addition, there is no critical degradation in proposed MOMP-based CE compared to conventional OMP where both methods are using oversampling ($X = 4$). The MOMP has less complexity without sacrificing the BER performance.

The simulation results have the same expectation in the case of hilly terrain environment in Fig.5.10. The simulation parameters is the same with the TU6

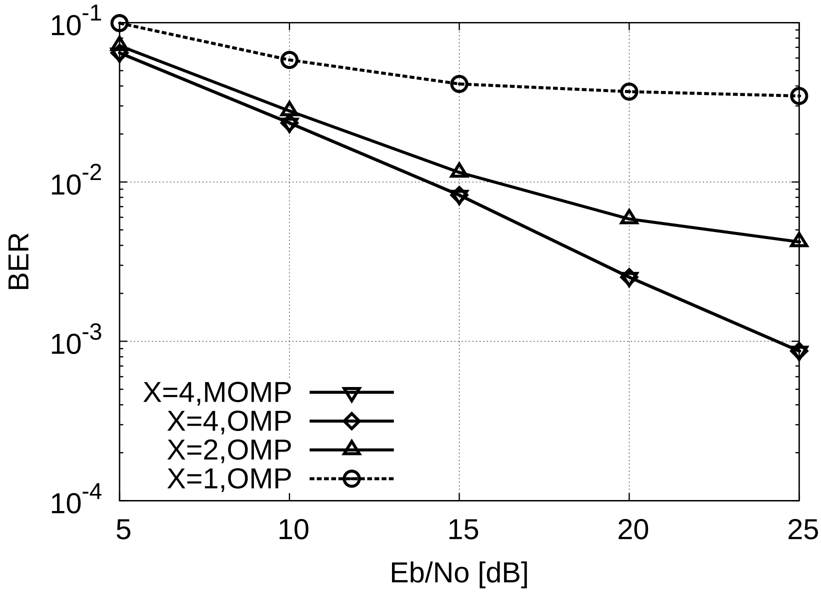

Figure 5.9: BER performance in TU6 channel

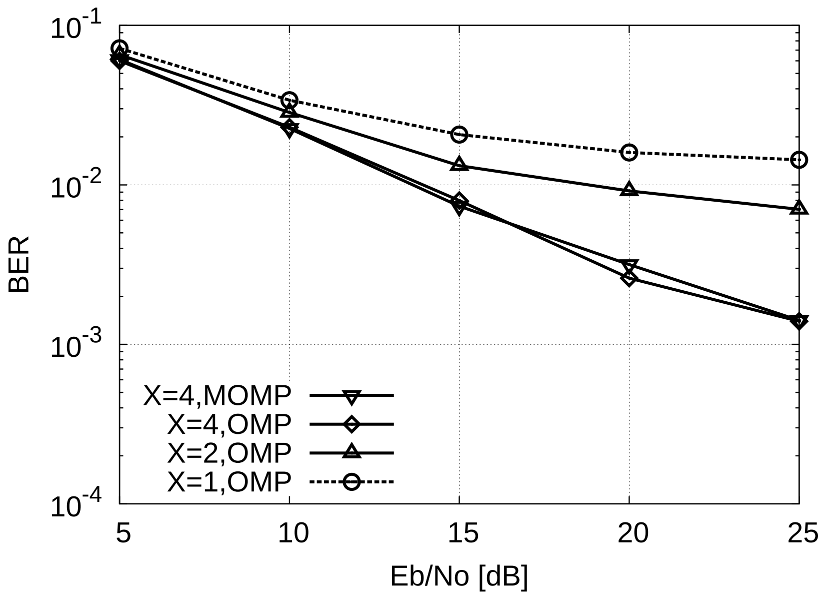

Figure 5.10: BER performance in hilly terrain

channel except that the guard interval was increased. The BER performance in hilly terrain shows that the virtual oversampling ($X = 2, X = 4$) has less error compared to non-virtual oversampling ($X = 1$).

5.4 Summary

This chapter discusses a fractional delay issue that exist in time domain based channel estimation. The fractional delay will leak the energy path to the other taps of CIR resulting for the CIR to be non-sparse. Because the CIR is no longer sparse, the measurement of CIR impulse position using CS is no longer accurate.

In order to mitigate the impact of fractional delay, a virtual oversampling at the receiver was proposed to guarantee successful reconstruction of the unknown CIR. The proposed system can avoid the increase of bandwidth during transmission since virtual oversampling carries out at the receiver side only.

During estimation of CIR, the OMP is applied to estimate the position and gain of each impulse of CIR. However, it was found out that the time delay of each path changes slowly compared to the gain of each path. Because of this assumption, a modified OMP was proposed to reduce the computational complexity in estimating the CIR without sacrificing the BER performance. The MOMP is composed of two parts. The first part will estimate both delay and gain of first symbol arrival using OMP, while the second part will only estimate the gain of succeeding symbol arrivals using least square.

The NMSE and BER performance for different channel models verified that a system with virtual oversampling has better performance compared to a system without virtual oversampling. This suggest that virtual orversampling can mitigate the impact of fractional delay. In addition, the computational cost was also reduced using the proposed MOMP compared to the conventional OMP. The BER performance of MOMP is comparable to OMP even though the MOMP has less complexity compared to OMP.

6 Conclusion

Overtime, the DTTB system is always evolving and improving. On the other hand, the demand for higher transmission capacity is increasing to support the evolution of DTTB system. Several possible methods and techniques were studied to improve the transmission capacity and efficiency in the field of wireless communication. An example is the application of LDM and compressed sensing. In this dissertation, the researcher considered an implementation of LDM for migration of next generation DTTB system. The LDM offers additional transmission capacity because multiple information can be transmitted at the same time using the same frequency spectrum resources. The researcher also consider an implementation compressed sensing for channel estimation because compressed sensing only requires less pilots and the bit error rate is within acceptable rate.

The first contribution in Chapter 3 is about increasing the transmission capacity to be used for migration of next generation DTTB system. In this chapter, we implement Layered Division Multiplexing to transmit additional data together with ISDB-T. The researcher proposes to reuse the ISDB-T data and use the additional data to scale up into 4K resolution for next generation DTTB system. The whole system implements space time block coding in a single frequency network to increase the diversity gain. Since the LDM transmission capacity exceeds the minimum requirement to establish a 4K TV transmission, the researcher proposes a partial LDM to lessen the interference between primary and secondary layer. With partial LDM, the BER performance will be less error compared to conventional full LDM. With the application of STBC-SFN, the BER performance will be lesser as the number of antenna increases.

In order to have better transmission reliability, channel estimation is necessary for DTTB system. Using CS for channel estimation can improve the transmission reliability with high transmission efficiency because CS only requires less pilots for channel estimation. However, CS requires high complexity because of huge number of OFDM subcarriers of DTTB to be estimated. In addition, the CS requires L_p norm to obtain the sparse solution. In Chapter 4, the dissertation presented that time domain CE can reduce the complexity of CS because it only requires the estimation of channel impulse response instead of channel frequency response for all OFDM subcarriers. Instead of using L_p norm, this dissertation uses greedy algorithm such as Orthogonal Matching Pursuit because it has less complexity compared to L_p norm.

The second contribution of this dissertation is presented in Chapter 5. It is said that time domain CE can reduce the complexity of CS, however, fractional delay issue arises due to non-synchronization between the transmitter and receiver. In Chapter 5, the researcher discusses the impact of fractional delay where the CIR is no longer sparse and the CS can no longer estimate the CIR properly. One of the solution to lessen the impact of fractional delay is to implement oversampling. However, oversampling can increase the transmission bandwidth and the ISDB-T bandwidth is limited to only 6MHz. In this chapter, the research proposes a virtual oversampling to avoid increase of bandwidth and to lessen the impact of fractional delay. In addition, the researcher modified the Orthogonal Matching Pursuit for further complexity reduction. The NMSE and BER performance shows that the virtual oversampling has less error compared to a system without oversampling. This suggest that the virtual oversampling can mitigate the impact of fractional delay. Another conclusion we can get is the NMSE and BER performance of Modified Orthogonal Matching pursuit is comparable to Orthogonal Matching Pursuit even though the researcher reduce the complexity of OMP.

Acknowledgements

First and foremost, I would like to thank the almighty God for given me the knowledge and strength to reach my dreams.

I would like to thank my supervisor Professor Minoru Okada for his support and guidance during my research in Master and Doctoral course. And also for my thesis co-supervisors Professor Kenji Sugimoto, Associate Professor Takeshi Higashino, Assistant Professor Duong Quang Thang, and Assistant Professor Yafei Hou for their comments and discussions to improve my research.

My appreciation to the Ministry of Education, Culture, Sports, Science & Technology in Japan (MEXT) for the scholarship grant and financial support of my Master Degree and Doctoral Course in Japan.

My acknowledgement to the members of the Network Systems Laboratory for their helpful suggestions and comments of my research progress. To my friends in Japan and Philippines for enjoyable and good moments we have together. Also I specially thank the international community in NAIST for the help and support during my stay here in Japan.

Most of all, to my parents for their support in every decision of my life. Thank you for the encouragement and inspiration you gave me.

References

[1] DTV Status. http://www.dtvstatus.net/.

[2] Association of Radio Industries and Businesses. Transmission system for digital terrestrial television broadcasting, ARIB STD-B31 version 1.6-E2. 2005.

[3] R. Paderna, D. Q. Thang, Y. Hou, T. Higashino, and M. Okada. Diversity gain analysis of SFN-STBC digital terrestrial TV system using dual polarized MIMO antenna. In *2016 IEEE International Symposium on Broadband Multimedia Systems and Broadcasting (BMSB)*, pages 1–4, June 2016.

[4] J. R. Ohm, G. J. Sullivan, H. Schwarz, T. K. Tan, and T. Wiegand. Comparison of the Coding Efficiency of Video Coding Standards-Including High Efficiency Video Coding (HEVC). *IEEE Transactions on Circuits and Systems for Video Technology*, 22(12):1669–1684, Dec 2012.

[5] J. J. van de Beek, O. Edfors, M. Sandell, S. K. Wilson, and P. O. Borjesson. On channel estimation in OFDM systems. In *1995 IEEE 45th Vehicular Technology Conference. Countdown to the Wireless Twenty-First Century*, volume 2, pages 815–819 vol.2, Jul 1995.

[6] International Telecommunication Union. Measuring the Information Society 2013. Geneva, 2013.

[7] European Broadcasting Union. Digital Video Broadcasting (DVB) framing structure, channel coding and modulation for digital terrestrial television. ETSI EN 300 744 V1.6.1, 2009,.

[8] Advanced Television Systems Committee Inc. A/53: ATSC Digital Television Standard, Parts 1 - 6. 2007.

[9] Chinese National Standard GB 20600-2006. Framing Structure, Channel Coding and Modulation for Digital Television Terrestrial Broadcasting System.

[10] S. I. Park, J. Y. Lee, S. Myoung, L. Zhang, Y. Wu, J. Montalbán, S. Kwon, B. M. Lim, P. Angueira, H. M. Kim, N. Hur, and J. Kim. Low Complexity Layered Division Multiplexing for ATSC 3.0. *IEEE Transactions on Broadcasting*, 62(1):233–243, March 2016.

[11] R. J. M. Cramer, R. A. Scholtz, and M. Z. Win. Evaluation of an ultra-wide-band propagation channel. *IEEE Transactions on Antennas and Propagation*, 50(5):561–570, May 2002.

[12] A. F. Molisch. Ultrawideband propagation channels-theory, measurement, and modeling. *IEEE Transactions on Vehicular Technology*, 54(5):1528–1545, Sept 2005.

[13] N. Czink, X. Yin, H. OZcelik, M. Herdin, E. Bonek, and B. H. Fleury. Cluster Characteristics in a MIMO Indoor Propagation Environment. *IEEE Transactions on Wireless Communications*, 6(4):1465–1475, April 2007.

[14] L. Vuokko, V. M. Kolmonen, J. Salo, and P. Vainikainen. Measurement of Large-Scale Cluster Power Characteristics for Geometric Channel Models. *IEEE Transactions on Antennas and Propagation*, 55(11):3361–3365, Nov 2007.

[15] W. U. Bajwa, J. Haupt, A. M. Sayeed, and R. Nowak. Compressed Channel Sensing: A New Approach to Estimating Sparse Multipath Channels. *Proceedings of the IEEE*, 98(6):1058–1076, June 2010.

[16] D. L. Donoho. Compressed sensing. *IEEE Transactions on Information Theory*, 52(4):1289–1306, April 2006.

[17] M. Nagahara K. Hayashi and T. Tanaka. A User's Guide to Compressed Sensing for Communications Systems. *IEICE Transactions on Communications*, E96.B(3):685–712, 2013.

[18] R. Paderna, D. Q. Thang, Y. Hou, T. Higashino, and M. Okada. Low-Complexity Compressed Sensing-Based Channel Estimation With Virtual Oversampling for Digital Terrestrial Television Broadcasting. *IEEE Transactions on Broadcasting*, 63(1):82–91, March 2017.

[19] R. Paderna, T. Higashino, M. Okada, and T. Iwamatsu. Modified orthogonal matching pursuit based ISDB-T channel estimation over fractional delay channel. In *2014 14th International Symposium on Communications and Information Technologies (ISCIT)*, pages 336–340, Sept 2014.

[20] S. Weinstein and P. Ebert. Data Transmission by Frequency-Division Multiplexing Using the Discrete Fourier Transform. *IEEE Transactions on Communication Technology*, 19(5):628–634, October 1971.

[21] S.C. Yang. *OFDMA System Analysis and Design*. Artech House telecommunications library. Artech House, 2010.

[22] S. Saito, T. Shitomi, S. Asakura, A. Satou, M. Okano, K. Murayama, and K. Tsuchida. 8K Terrestrial Transmission Field Tests Using Dual-Polarized MIMO and Higher-Order Modulation OFDM. *IEEE Transactions on Broadcasting*, 62(1):306–315, March 2016.

[23] A. Mattsson. Single frequency networks in DTV. *IEEE Transactions on Broadcasting*, 51(4):413–422, Dec 2005.

[24] V. Tarokh, H. Jafarkhani, and A. R. Calderbank. Space-time block coding for wireless communications: performance results. *IEEE Journal on Selected Areas in Communications*, 17(3):451–460, Mar 1999.

[25] S. M. Alamouti. A simple transmit diversity technique for wireless communications. *IEEE Journal on Selected Areas in Communications*, 16(8):1451–1458, Oct 1998.

[26] Ministry of Internal Affairs and Communications. https://www.tele.soumu.go.jp.

[27] L. Zhang, W. Li, Y. Wu, X. Wang, S. I. Park, H. M. Kim, J. Y. Lee, P. Angueira, and J. Montalban. Layered-Division-Multiplexing: Theory and Practice. *IEEE Transactions on Broadcasting*, 62(1):216–232, March 2016.

[28] T. Cover. Broadcast channels. *IEEE Transactions on Information Theory*, 18(1):2–14, Jan 1972.

[29] A. Schertz and C. Weck. Hierarchical modulation - the transmission of two independent DVB-T multiplexes on a single frequency. *EBU Technical Review*, April 2003.

[30] Hong Jiang and P. A. Wilford. A hierarchical modulation for upgrading digital broadcast systems. *IEEE Transactions on Broadcasting*, 51(2):223–229, June 2005.

[31] S. I. Park, G. Lee, H. M. Kim, N. Hur, S. Kwon, and J. Kim. ADT-Based UHDTV Transmission for the Existing ATSC Terrestrial DTV Broadcasting. *IEEE Transactions on Broadcasting*, 61(1):105–110, March 2015.

[32] R. Paderna, Y. Hou, and M. Okada. Space-time block coding in a single frequency network with partial layered division multiplexing for DTV terrestrial systems. *ITE Tech. Rep., BCT2017-48*, 41(11):37–40, March 2017.

[33] D. Gómez-Barquero and O. Simeone. LDM versus FDM/TDM for Unequal Error Protection in Terrestrial Broadcasting Systems: An Information-Theoretic View. *IEEE Transactions on Broadcasting*, 61(4):571–579, Dec 2015.

[34] G. J. Sullivan, J. R. Ohm, W. J. Han, and T. Wiegand. Overview of the High Efficiency Video Coding (HEVC) Standard. *IEEE Transactions on Circuits and Systems for Video Technology*, 22(12):1649–1668, Dec 2012.

[35] IT++. http://www.itpp.sourceforge.net.

[36] COST207. Digital land mobile communications. *Commission of the European Communities, Directorate General Communications, Information Industries and Innovation*, pages 135–147, 1989.

[37] I. Barhumi, G. Leus, and M. Moonen. Optimal training design for MIMO OFDM systems in mobile wireless channels. *IEEE Transactions on Signal Processing*, 51(6):1615–1624, June 2003.

[38] M. K. Ozdemir and H. Arslan. Channel estimation for wireless OFDM systems. *IEEE Communications Surveys Tutorials*, 9(2):18–48, Second 2007.

[39] K. Hayashi, M. Sakai, T. Kamenosono, and M. Kaneko. Compressed sensing based channel estimation for uplink OFDMA systems. In *Signal and Information Processing Association Annual Summit and Conference (APSIPA), 2014 Asia-Pacific*, pages 1–7, Dec 2014.

[40] R. Paderna, M. Okada, T. Higashino, and H. Furudate. Modified Matching Pursuit based channel estimation for ISDB-T. In *2013 International Symposium on Intelligent Signal Processing and Communication Systems*, pages 119–124, Nov 2013.

[41] Z. Ma and M. Okada. Impulsive Noise Suppression for ISDB-T Receivers Based on Adaptive Window Function. *IEICE Transactions on Fundamentals of Electronics, Communications and Computer Sciences*, E94.A(11):2237–2245, 2011.

[42] C. R. Berger, Z. Wang, J. Huang, and S. Zhou. Application of compressive sensing to sparse channel estimation. *IEEE Communications Magazine*, 48(11):164–174, November 2010.

[43] S. F. Cotter and B. D. Rao. Sparse channel estimation via matching pursuit with application to equalization. *IEEE Transactions on Communications*, 50(3):374–377, Mar 2002.

[44] J. Oliver, R. Aravind, and K. M. M. Prabhu. Sparse channel estimation in ofdm systems by threshold-based pruning. *Electronics Letters*, 44(13):830–832, June 2008.

[45] J. A. Tropp and A. C. Gilbert. Signal Recovery From Random Measurements Via Orthogonal Matching Pursuit. *IEEE Transactions on Information Theory*, 53(12):4655–4666, Dec 2007.

[46] R. E. Carrillo, L. F. Polania, and K. E. Barner. Iterative algorithms for compressed sensing with partially known support. In *2010 IEEE International Conference on Acoustics, Speech and Signal Processing*, pages 3654–3657, March 2010.

[47] E. J. Candes and M. B. Wakin. An Introduction To Compressive Sampling. *IEEE Signal Processing Magazine*, 25(2):21–30, March 2008.

[48] E. J. Candes and T. Tao. Decoding by linear programming. *IEEE Transactions on Information Theory*, 51(12):4203–4215, Dec 2005.

[49] E. J. Candes, J. Romberg, and T. Tao. Robust uncertainty principles: exact signal reconstruction from highly incomplete frequency information. *IEEE Transactions on Information Theory*, 52(2):489–509, Feb 2006.

[50] J. Haupt, L. Applebaum, and R. Nowak. On the Restricted Isometry of deterministically subsampled Fourier matrices. In *2010 44th Annual Conference on Information Sciences and Systems (CISS)*, pages 1–6, March 2010.

[51] S. G. Mallat and Zhifeng Zhang. Matching pursuits with time-frequency dictionaries. *IEEE Transactions on Signal Processing*, 41(12):3397–3415, Dec 1993.

[52] R. Paderna, D. Q. Thang, Y. Hou, T. Higashino, and M. Okada. Compressed Sensing based Channel Impulse Response Estimation for Space Time Block Coding Single Frequency Network in DTV System. *ITE Technical Report*, 40(4):21–24, Feb 2016.

[53] R. Paderna. Low Complexity Channel Estimation for ISDB-T using Modified Orthogonal Matching Pursuit (Master Thesis), NAIST, March 2015.

[54] Y. Wang, L. Li, P. Zhang, and Z. Liu. Channel estimation for OFDM systems in non-sample-spaced multipath channels. *Electronics Letters*, 45(1):66–68, January 2009.

[55] R. Paderna, T. Higashino, and M. Okada. Improved channel estimation for ISDB-T using Modified Orthogonal Matching Pursuit over fractional de-

lay TU6 channel. In *Signal and Information Processing Association Annual Summit and Conference (APSIPA), 2014 Asia-Pacific*, pages 1–5, Dec 2014.

[56] B. Peng, P. S. Rossi, H. Dong, and K. Kansanen. Time-Domain Oversampled OFDM Communication in Doubly-Selective Underwater Acoustic Channels. *IEEE Communications Letters*, 19(6):1081–1084, June 2015.

[57] C. Tepedelenlioglu and R. Challagulla. Low-complexity multipath diversity through fractional sampling in OFDM. *IEEE Transactions on Signal Processing*, 52(11):3104–3116, Nov 2004.

[58] J. Wu and Y. R. Zheng. Oversampled Orthogonal Frequency Division Multiplexing in Doubly Selective Fading Channels. *IEEE Transactions on Communications*, 59(3):815–822, March 2011.

[59] L. Dai, J. Wang, Z. Wang, P. Tsiaflakis, and M. Moonen. Spectrum- and Energy-Efficient OFDM Based on Simultaneous Multi-Channel Reconstruction. *IEEE Transactions on Signal Processing*, 61(23):6047–6059, Dec 2013.

[60] R. Chen and K. B. Letaief. Channel estimation for space time coded OFDM systems in non-sample-spaced multipath channels. In *2002 IEEE Wireless Communications and Networking Conference Record. WCNC 2002 (Cat. No.02TH8609)*, volume 1, pages 61–66 vol.1, Mar 2002.

[61] E. Candes and T. Tao. The Dantzig selector: Statistical estimation when p is much larger than n. *ArXiv Mathematics e-prints*, June 2005.

[62] R. Niazadeh, M. Babaie-Zadeh, and C. Jutten. On the Achievability of Cramer-Rao Bound in Noisy Compressed Sensing. *IEEE Transactions on Signal Processing*, 60(1):518–526, Jan 2012.

Publication List

Journal

J1. Ryan Paderna, Yafei Hou, Duong Quang Thang, Takeshi Higashino, and Minoru Okada, "Partial Layered Division Multiplexing with STBC for ISDB-T and Next Generation DTTB Systems," in *Special Section on Advanced Multimedia Transmission Technology and Its Application : ITE Transactions on Media Technology and Applications*, vol. 6, no. 1, pp. 98-109, January 2018. [Corresponds to Chapter 3]

J2. Ryan Paderna, Duong Quang Thang, Yafei Hou, Takeshi Higashino, and Minoru Okada, "Low-Complexity Compressed Sensing-Based Channel Estimation With Virtual Oversampling for Digital Terrestrial Television Broadcasting," in *IEEE Transactions on Broadcasting*, vol. 63, no. 1, pp. 82-91, March 2017. [Corresponds to Chapter 5]

International Conferences (Peer Review)

I1. Ryan Paderna, Duong Quang Thang, Yafei Hou, Takeshi Higashino, and Minoru Okada, "Diversity gain analysis of SFN-STBC digital terrestrial TV system using dual polarized MIMO antenna," in *2016 IEEE International Symposium on Broadband Multimedia Systems and Broadcasting (BMSB)*, pp. 1-4, Nara, Japan, June 2016. [Corresponds to Chapter 2 and 4]

I2. Ryan Paderna, Yafei Hou, Takeshi Higashino, and Minoru Okada, "Improved compressed sensing based channel estimation for terrestrial DTV using auxiliary pilot channel," in *2015 15th International Symposium on Communications and Information Technologies (ISCIT)*, pp. 213-216, Nara, Japan, Oct. 2015. [Corresponds to Chapter 2 and 4]

Domestic Conferences (Non Peer Review)

D1. Ryan Paderna, Yafei Hou, and Minoru Okada, "Space-Time Block Coding in a Single Frequency Network with partial Layered Division Multiplexing for DTV Terrestrial System," in *ITE Technical Report*, vol. 41, no. 11, BCT2017-48, pp. 37-40, Nagasaki, Japan, March 2017. [Corresponds to Chapter 3]

D2. Ryan Paderna, Duong Quang Thang, Yafei Hou, Takeshi Higashino, and Minoru Okada, "Time Domain Compressed Sensing based Channel Estimation in Fast Fading Channel with Fractional Delay," in *ITE Technical Report*, vol. 40, no. 35, BCT2016-74, pp. 5-8, Aomori, Japan, Oct. 2016. [Corresponds to Chapter 5]

D3. Ryan Paderna, Duong Quang Thang, Yafei Hou, Takeshi Higashino, and Minoru Okada, "Compressed Sensing based Channel Impulse Response Estimation for Space Time Block Coding Single Frequency Network in DTV System," in *ITE Technical Report*, vol. 40, no. 4, pp. 21-24, Otaru, Japan, Feb. 2016. [Corresponds to Chapter 4]